

LETTER TO THE EDITOR

Discovery of two cyano derivatives of acenaphthylene ($C_{12}H_8$) in TMC-1 with the QUIJOTE line survey[★]

J. Cernicharo¹, C. Cabezas¹, R. Fuentetaja¹, M. Agúndez¹, B. Tercero^{2,3}, J. Janeiro⁴, M. Juanes⁵, R. I. Kaiser⁶, Y. Endo⁷, A. L. Steber⁵, D. Pérez⁴, C. Pérez⁵, A. Lesarri⁵, N. Marcelino^{2,3}, P. de Vicente²

¹ Dept. de Astrofísica Molecular, Instituto de Física Fundamental (IFF-CSIC), C/ Serrano 121, 28006 Madrid, Spain.
e-mail: jose.cernicharo@csic.es

² Centro de Desarrollos Tecnológicos, Observatorio de Yebes (IGN), 19141 Yebes, Guadalajara, Spain.

³ Observatorio Astronómico Nacional (OAN, IGN), C/ Alfonso XII, 3, 28014, Madrid, Spain.

⁴ Centro Singular de Investigación en Química Biológica e Materiais Moleculares (CiQUS) and Departamento de Química Orgánica, Universidade de Santiago de Compostela, 15782 Santiago de Compostela, Spain

⁵ Departamento de Química Física y Química Inorgánica, Facultad de Ciencias-I.U. CINQUIMA, Universidad de Valladolid, 47011 Valladolid, Spain

⁶ Department of Chemistry, University of Hawaii at Manoa, Honolulu, HI 96822, USA

⁷ Department of Applied Chemistry, Science Building II, National Yang Ming Chiao Tung University, 1001 Ta-Hsueh Rd., Hsinchu 300098, Taiwan

Received 10 September 2024; accepted 18 September 2024

ABSTRACT

We report the discovery in TMC-1 of two cyano derivatives of the PAH acenaphthylene ($C_{12}H_8$). We have found two series of lines with the QUIJOTE line survey that we assign to 1- $C_{12}H_7CN$ and 5- $C_{12}H_7CN$. For the 1-isomer, we have detected and assigned 173 rotational transitions with J up to 46 and K_a up to 9, corresponding to 107 independent frequencies. For the 5-isomer, the identification is based on 56 individual lines, corresponding to 117 rotational transitions with J up to 40 and K_a up to 8. Identification of the carriers was achieved through a careful analysis of the derived rotational constants, which permit us to focus on molecules larger than naphthalene but smaller than anthracene and phenanthrene. Moreover, the derived rotational constants indicate that the species are planar; this allows us to discard derivatives of fluorene and acenaphthene, which are non-planar species. Quantum chemical calculations and subsequent chemical synthesis of these molecules, as well as the observation of their rotational transitions in the laboratory, unequivocally support our identifications. We also confirm, via a robust line-by-line detection, the previous claimed detection of 1- and 2- cyanonaphthalene, which were obtained through statistical stacking techniques. The column densities of 1- and 5-cyanoacenaphthylene are $(9.5 \pm 0.9) \times 10^{11} \text{ cm}^{-2}$, while those of 1- and 2-cyanonaphthalene are $(5.5 \pm 0.5) \times 10^{11} \text{ cm}^{-2}$. Hence, it seems that acenaphthylene could be a factor of 1.7 more abundant than naphthalene. These results support a scenario in which PAHs grow in cold dark clouds based on fused five- and six-membered carbon rings.

Key words. molecular data — line: identification — ISM: molecules — ISM: individual (TMC-1) — astrochemistry

1. Introduction

The QUIJOTE¹ ultrasensitive line survey (Cernicharo et al. 2021a) has provided the detection of more than 60 molecular species in the last four years. Some of them are very polar molecules with relatively low abundances such as the 16 S-bearing species discovered in TMC-1 (Cernicharo et al. 2024), the radicals H_2C_3N and H_2C_4N (Cabezas et al. 2021, 2023), and the double-cyanide derivatives of methane ($NCCH_2CN$) and ethylene ($NCCHCHCN$) (Agúndez et al. 2024). Nevertheless, one of the most significant results of QUIJOTE is the discovery, through the standard method of line-by-line detection, of low-dipole but very abundant pure hydrocarbons, such as

CH_2CHCCH (Cernicharo et al. 2021b), $o\text{-}C_6H_4$ (Cernicharo et al. 2021a), $CH_2CCHCCH$ (Cernicharo et al. 2021c), $c\text{-}C_5H_6$, and $c\text{-}C_9H_8$ (cyclopentadiene and indene; Cernicharo et al. 2021d), the radical H_2CCCH (Agúndez et al. 2021, 2022), the long carbon chain CH_2CCHC_4H (Fuentetaja et al. 2022), and fulvenallene ($c\text{-}C_5H_5CCH_2$; Cernicharo et al. 2022). These neutrals, together with some cations, such as $l\text{-}C_3H_3^+$ (Silva et al. 2023), certainly play an important role in the growth of larger hydrocarbons and PAHs in TMC-1 (Cernicharo et al. 2022).

Indene is the only polycyclic aromatic hydrocarbon (PAH) discovered directly from its rotational spectrum (Cernicharo et al. 2021d). However, the cyano derivatives of benzene and naphthalene have been reported in TMC-1 using stacking techniques with the GOTHAM line survey (McGuire et al. 2018, 2021). It is not clear yet how these PAHs are formed in a cold dark cloud. It is unlikely that these molecules arise from a reservoir of PAHs existing since the early stages of the cloud, because these relatively small PAHs would not have survived the diffuse cloud stage. Moreover, the spatial distribution of benzonitrile is identical to that of cyanopolynes and other molecular species

[★] Based on observations carried out with the Yebes 40m telescope (projects 19A003, 20A014, 20D023, 21A011, 21D005, and 23A024). The 40m radio telescope at Yebes Observatory is operated by the Spanish Geographic Institute (IGN, Ministerio de Transportes, Movilidad y Agenda Urbana).

¹ Q-band Ultrasensitive Inspection Journey to the Obscure TMC-1 Environment

(Cernicharo et al. 2023a). Hence, the observational evidence points towards a bottom-up formation process for these species in TMC-1. The chemical ingredients that form PAHs are the carbon chains, radicals, and cations that have been detected with QUIJOTE and mentioned above. However, the detailed chemical routes for the growth of PAHs are only beginning to emerge (Kaiser & Hansen 2021; Cernicharo et al. 2022). Taking into account the large abundances of indene and those inferred for benzene and naphthalene from their cyanide derivatives, it is clear that just a few reactions are involved in their production. Unfortunately, these reactions are still missing in our chemical networks. Consequently, it is highly important to detect more PAHs in order to provide additional clues as to their chemistry.

In this work, we present the discovery from the QUIJOTE data of two cyano derivatives of acenaphthylene ($c\text{-C}_{12}\text{H}_8$), which is composed of three fused carbon rings (two six-membered and one five-membered). We also confirm the previous identification of cyanonaphthalenes (McGuire et al. 2021) through a robust line-by-line detection. The derived abundances indicate that cyanoacenaphthylenes are ~ 1.7 more abundant than cyanonaphthalenes. This result suggests that bigger PAHs in TMC-1 probably consist of a mixture of fused five- and six-membered carbon rings. We discuss possible formation routes for these molecules in cold clouds, such as TMC-1.

2. Observations

The observational data presented in this work are part of the QUIJOTE spectral line survey (Cernicharo et al. 2021a) in the Q-band towards TMC-1(CP) ($\alpha_{J2000} = 4^{\text{h}}41^{\text{m}}41.9^{\text{s}}$ and $\delta_{J2000} = +25^{\circ}41'27.0''$), which was performed at the Yebes 40m radio telescope. This survey was carried out using a receiver built within the Nanocosmos project² consisting of two cooled high-electron-mobility-transistor (HEMT) amplifiers covering the 31.0-50.3 GHz band with horizontal and vertical polarization. Fast Fourier transform spectrometers (FFTSs) with 8×2.5 GHz and a spectral resolution of 38.15 kHz provide the whole coverage of the Q-band in both polarizations. Receiver temperatures are 16 K at 32 GHz and 30 K at 50 GHz. The experimental setup is described in detail by Tercero et al. (2021).

All observations were performed using frequency-switching observing mode with a frequency throw of 10 and 8 MHz. The total observing time on the source for data taken with frequency throws of 10 MHz and 8 MHz is 465 and 737 hours, respectively. Hence, the total observing time on source is 1202 hours. The QUIJOTE sensitivity varies between 0.08 mK at 32 GHz and 0.2 mK at 49.5 GHz. A detailed description of the line survey and the data-analysis procedure are provided in Cernicharo et al. (2021a, 2022). The main beam efficiency can be given across the Q band as $B_{\text{eff}} = 0.797 \exp[-(\nu(\text{GHz})/71.1)^2]$. The forward telescope efficiency is 0.97. The telescope beam size at half power intensity is $54.4''$ at 32.4 GHz and $36.4''$ at 48.4 GHz. The absolute calibration uncertainty is 10%. The data were analysed with the GILDAS package³.

3. Results

Line identification in this work was performed using the MADEX code (Cernicharo 2012), in conjunction with the CDMS and JPL catalogues (Müller et al. 2005; Pickett et al. 1998). The intensity scale used in this study is the antenna

temperature (T_A^*). Consequently, the telescope parameters and source properties were used when modelling the emission of the different species in order to produce synthetic spectra on this temperature scale. In this work, we assumed a velocity for the source relative to the local standard at rest of 5.83 km s^{-1} (Cernicharo et al. 2020). The source was assumed to be circular with a uniform brightness temperature and a radius of $40''$ (Fossé et al. 2001).

3.1. A peculiar way to search for PAHs

We would like to start by introducing the method we used to search for new PAHs. Although seemingly disconnected, the story deserves to be told. When we detected the anion C_7N^- (Cernicharo et al. 2023b), we searched intensively for C_7N . Quantum chemical calculations by Botschwina et al. (1999) predicted an electronic ground state $^2\Pi$ with a moderate dipole moment of 1 D. However, due to the possible admixing of the ground state with a low-lying $^2\Sigma$ state, which has a dipole moment of ~ 3.6 D (Botschwina et al. 1999), the true value of the dipole moment could be between those of the two states, and in this case it could be detectable with our QUIJOTE data. The rotational constant of C_7N is predicted to be ~ 585 MHz. If the electronic ground state is $^2\Pi$, then the quantum numbers should be half integers. Our automatic programs to search for harmonic relations indicate 12 lines in very good harmonic relation with J half integers and $B_{\text{eff}} = 580.987$ MHz and $D_{\text{eff}} = 4.94$ Hz. Hereafter, we refer to these half-integer quantum numbers as J^* . This was a very exciting result, pointing towards the presence of C_7N in TMC-1. However, all these harmonically related lines could be easily identified with the MADEX catalogue with $K_a = 0, 1$, $J_u = J^* - 1/2$ transitions of 1-cyanonaphthalene (see Table A.1). These lines are shown in Fig. A.1, which is based on a modified Loomis-Wood diagram (Loomis & Wood 1928). Details of the confirmation of cyanonaphthalenes and of the harmonic relation with J half integers for a - and b -type $K_a = 0, 1$ transitions are given in Appendix A.

We verified that this peculiarity of the $K_a = 0, 1$ lines also applies —with some variations due to the value of the rotational constants and to the values of the dipole moment components— to many other PAHs such as indene, fluorene, cyanoanthracene, and cyanophenanthrene among others. For any oblate asymmetric rotor, pairing of lines will occur for high- J ; first for $K_c = J$, and then for $K_c = J-1$ and so on, and the effective B will approach C . A detailed analysis of the asymptotic behaviour of the energy levels of an asymmetric rotor is provided by Watson (2007). Consequently, visual inspection of the data following the method described in Appendix A allows us to easily detect the rotational transitions of heavy PAHs.

3.2. The series of lines B429 and B444

We searched using automatic and/or visual procedures for series of lines in harmonic relation with integer or half-integer quantum numbers. Once the series were found, we used the method described in the previous section and in Appendix A to visually explore the QUIJOTE data, searching for spectral patterns similar to those of 1- and 2-cyanonaphthalene. We discovered two series of lines harmonically related with half-integer quantum numbers. We quickly verified that these series could not be assigned to a species with quantum numbers $2J^*$ as all lines with even J would be missing. Hence, either we are detecting species

² <https://nanocosmos.iff.csic.es/>

³ <http://www.iram.fr/IRAMFR/GILDAS>

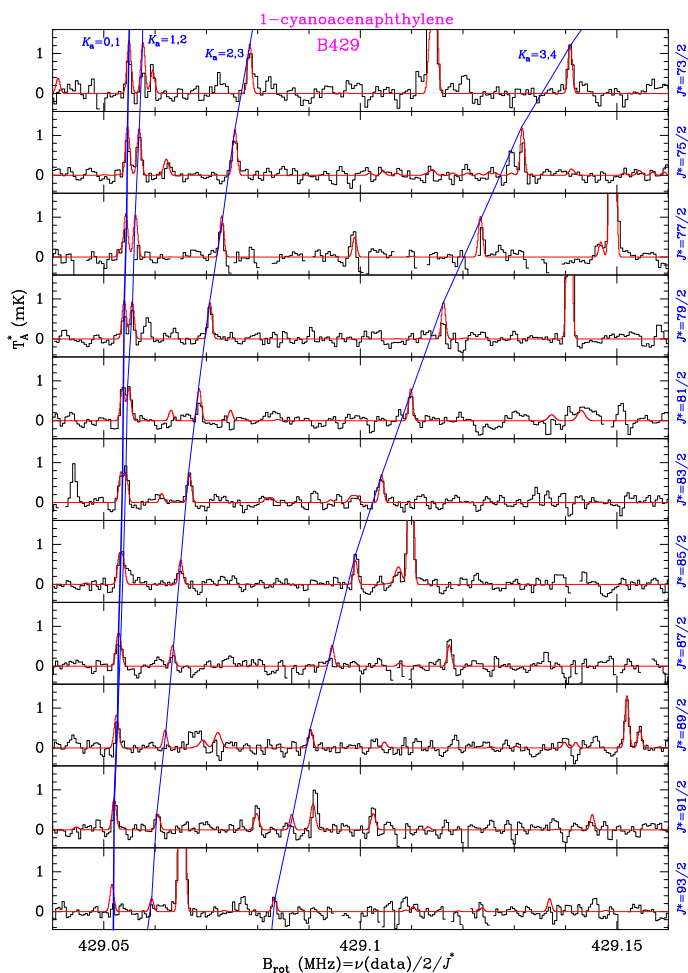


Fig. 1. Modified Loomis-Wood diagram of some of the observed lines of B429 (1-cyanoacenaphthylene). The abscissa corresponds to the value of the rotational constant, which has been fixed in this plot to values of between 429.040 and 429.160 MHz. The ordinate is the antenna temperature—corrected for atmospheric and telescope losses—in millikelvin. Each box presents the QUIJOTE data for frequencies $2 B_{rot} J^*$, where $J^* = J_u + 1/2$. The red line corresponds to the synthetic spectrum computed for TMC-1, including the rotational transitions of all molecular species detected with QUIJOTE, adopting for them the physical parameters derived in all previous works. This spectrum contains the rotational lines of the two isomers of cyanoacenaphthylene discovered in this paper. The rotational transitions of 1-cyanoacenaphthylene correspond to those connected through blue lines (see text). The blue line on the left side corresponds to the $K_a = 0, 1$ transitions that are harmonically related with half-integer quantum numbers.

in a $2^2\Pi$ state, or we are observing a similar case to that of 1- and 2-cyanonaphthalene.

The first series could be fitted with $B_{\text{eff}} = 429.0596 \pm 0.0003$ MHz and $D_{\text{eff}} = 1.81 \pm 0.07$ Hz, with J^* from $73/2$ to $93/2$. The standard deviation of the fit is 11.6 kHz. Hereafter, we refer to this series of lines as B429. Using the same kind of modified Loomis-Wood plot described above, we found additional series of lines at slightly higher frequencies than those of B429. The first four series of lines, including those of B429, are shown in Fig. 1. To facilitate their visual identification, they are connected by blue straight lines, similarly to the visualization of 1-cyanonaphthalene shown in Fig. A.1. The lines connected by the first blue line (left one) correspond to upper quantum numbers J_u , $K_a = 0, 1$, and $K_c = J_u$, where J_u for each panel is $J^* - 1/2$ (J^* is indicated at the right side of the panels). These lines are

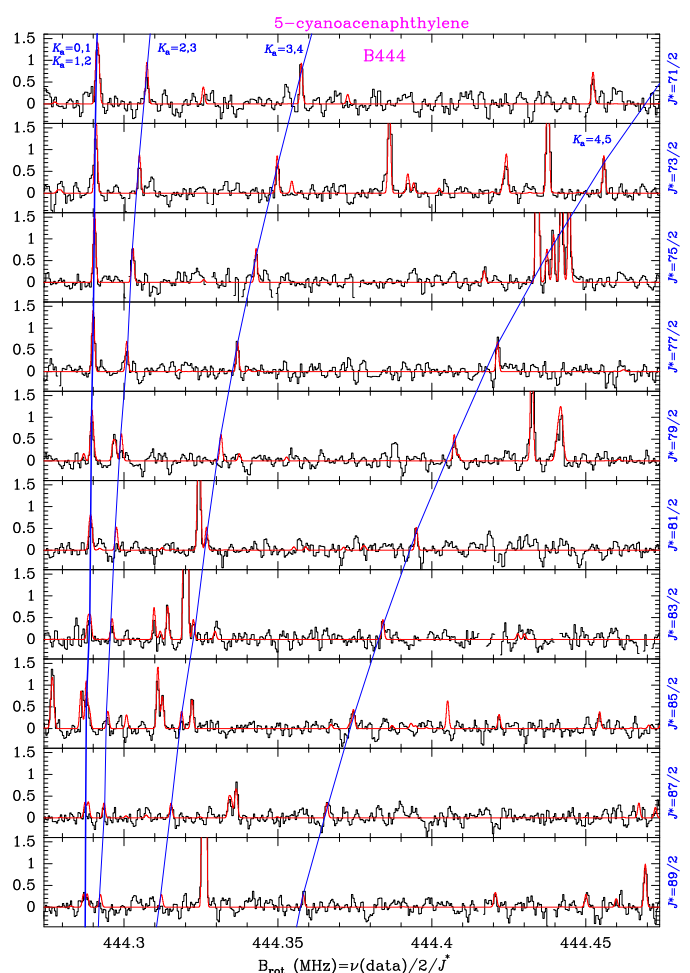


Fig. 2. Similar to Fig. 1 but for B444 (5-cyanoacenaphthylene). The range of B_{rot} is from 444.274 to 444.474 MHz.

those of B429 and are perfectly reproduced with the constants B_{eff} and D_{eff} derived above. The second blue line connects the transitions $J_u - 1$, $K_a = 1, 2$, and $K_c = J_u - 2$; it collapses to the first blue line for $J^* = 83/2$ ($J_u = 41$). The third blue line connects the transitions $J_u - 2$, $K_a = 2, 3$, and $K_c = J_u - 3$. All transitions are $\Delta J = +1$. Many additional series of lines related to B429 were found in our data involving up to a total of 107 independent frequencies. The derived line parameters are given in Table B.1. It is clear that all these lines belong to the progressions of an asymmetric molecule with integer quantum numbers $J_u = J^* - 1/2$ (J_u from 35 up to 46).

In summary, the lines of B429 belong to $K_a = 0, 1$ (the set of transitions connected by the first blue line). The other lines have values of K_a varying from 1 up to 9. It was relatively easy to assign the quantum numbers to the 107 observed lines (corresponding to 173 rotational transitions) and to derive from these frequencies the rotational constants given in Table 1. We used an A -reduced Hamiltonian (representation I') and the derived rotational constants are given in Table 1. Similar to the case of 1- and 2-cyanonaphthalene, the rotational constant C derived differs from B_{eff} by less than 0.002 MHz.

The second series of lines in harmonic relation with half-integer quantum numbers is shown in Fig. 2. The lines are connected by a straight vertical blue line and can be reproduced with

$B_{\text{eff}} = 444.298526 \pm 0.00024$ MHz and $D_{\text{eff}} = 2.848 \pm 0.077$ Hz, with J^* between 71/2 and 85/2. Hereafter, we refer to the carrier of these lines as B444. Additional series of lines are shown in Fig. 2; these are also connected by blue lines that are assigned to $K_a = 1, 2,$ and 3 lines of an asymmetric rotor, similarly to B429. The line parameters of all the observed lines are given in Table B.1. A total of 56 independent lines corresponding to 117 rotational transitions were assigned to B444. The rotational and distortion constants of B444 derived using an A -reduced Hamiltonian (representation I') are given in Table 1.

For both carriers, the a - and b -type transitions have a significant collapse for $K_a = 0, 1$ and 1, 2. However, if the b component of the dipole moment is large, then we can expect to detect individual b -type transitions, as in the case of 1- and 2- cyanonaphthalene (see Fig. A.2). We searched for these b -type transitions for B429 and B444 without success, which indicates that the rotational spectrum is dominated by a -type transitions, that is, that μ_b is significantly lower than μ_a .

3.3. Quantum chemical calculations and identification of 1- and 5-cyanoacenaphthylene

In order to search for the carriers of B429 and B444, we compared the derived rotational constants with those of other asymmetric species to get some insights in their structure. The derived rotational constants for B429 and B444 could be compatible with cyano (or CCH) derivatives of anthracene, phenanthrene, acenaphthene, fluorene, and acenaphthylene, among other species with three fused rings.

We can discard derivatives of anthracene and phenanthrene as the rotational constants of these species, before any derivation, are smaller than those of B429 and B444 (Baba et al. 2009; Kowaka et al. 2012). To bolster our confidence in this conclusion, we performed quantum chemical calculations (see Appendix C) for all cyano derivatives of anthracene (see Table C.2) and phenanthrene (see Table C.3). None of these species, which are depicted in Fig. C.1 and C.2, can fit our rotational constants.

We can also discard non-planar molecules, as the derived C rotational constant for B429 and B444 is almost identical to $(A \times B)/(A + B)$, that is, the derived inertial defect is small or compatible with that of cyano derivatives of planar PAHs (see e.g. McNaughton et al. 2018). This allows us to discard cyano or ethylenic derivatives of indene, fluorene, and acenaphthene as possible carriers of our lines, as these species have large inertial defects due to the presence of one or two pairs of hydrogen atoms out of the plane of the molecule. Fluorene and acenaphthene have been observed in the laboratory by Thorwirth et al. (2007), and the cyano derivatives of fluorene have also been observed (Cabezas et al. 2024). Rotational constants for these species, together with values obtained from our quantum chemical calculations for CN derivatives of acenaphthene, are given in Tables C.4 and C.5. Indene derivatives have been studied in detail in the laboratory by Sita et al. (2022), and their rotational constants do not match those of B429 and B444. Doubly cyano derivatives of naphthalene, which are depicted in Fig. C.4, can also be discarded as carriers of our lines as their rotational constants are far from those of B429 and B444 (see Appendix C and Table C.6).

Finally, we consider the cyano derivatives of acenaphthylene ($C_{12}H_8$), a PAH that has been studied in the laboratory by Thorwirth et al. (2007) and that is planar (see central structure in Fig. 3). The rotational constants derived in the laboratory for this species are compared to those derived through our quantum chemical calculations in Table C.1. Four possible cyano deriva-

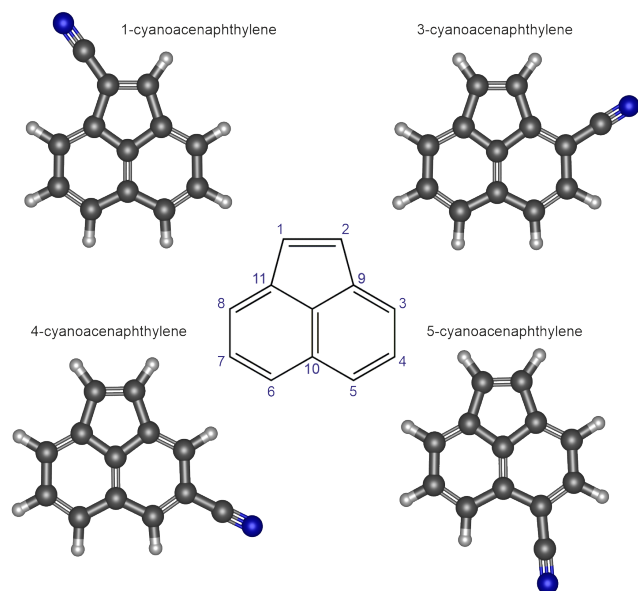


Fig. 3. Chemical structure of acenaphthylene (center design) and its cyano derivatives. The numbers label the nitrile substitution positions of the four possible isomers of cyanoacenaphthylene. The isomers detected in this work are 1-CNACY and 5-CNACY, which correspond to B429 and B444, respectively.

tives can be obtained for this species. The structure of the mother molecule and of its CN derivatives is shown in Fig. 3. Hereafter, we refer to the CN derivatives of acenaphthylene as n -CNACY ($n=1, 3, 4$ or 5). Our quantum chemical calculations indicate that 1-CNACY can be identified with B429 and that B444 can be assigned to 5-CNACY. The predicted rotational constants for the four isomers of CNACY ($n-C_{12}H_7CN$; $n=1, 3, 4,$ and 5) are given in Table 1.

In order to fully confirm the identification of B429 and B444 with 1-CNACY and 5-CNACY, we synthesized them in the chemical laboratory (see Appendix D) and observed their rotational spectrum in the microwave laboratory (see Appendix E). The resulting molecular parameters are given in Tables E.1 and E.2. The rotational constants derived in space for B429 agree with those of 1-CNACY (see Table E.1), and those of B444 are in perfect agreement with those of 5-CNACY (see Table E.2). Hence, we firmly conclude that we have detected, for the first time in space, two of the cyano derivatives of the PAH acenaphthylene. This is the first time that a 3-fused carbon ring is detected in space. Moreover, these are the first PAHs that are fully characterised from astronomical data prior to any laboratory information on its rotational spectrum. These molecules contain 21 atoms and are, apart from the fullerenes, the largest species found in space. We find no evidence in our data for the 3-CNACY and 4-CNACY; moreover, they cannot be produced in the laboratory following the procedure described in Appendix D.

4. Discussion

In order to derive column densities for the two cyanide derivatives of acenaphthylene, we assumed that these species are close to thermalisation, $T_{\text{rot}} = 9$ K, that molecular emission follows that of C_6H_5CN (Cernicharo et al. 2023a), and that it can be simplified, as in all our previous analyses, as a source of uniform brightness temperature of 80'' in diameter. With these assump-

Table 1. Molecular constants of the cyano isomers of acenaphthylene derived from QUIJOTE data (representation A I').

Parameter	1-CNACY ^a	B429 (TMC-1)	3-CNACY ^a	4-CNACY ^a	5-CNACY ^a	B444 (TMC-1)
A (MHz)	1271.64	1272.1707(19)	1476.89	1451.83	1248.93	1246.5874(75)
B (MHz)	647.47	647.27938(19)	608.98	565.62	688.66	690.1787(24)
C (MHz)	429.03	429.06155(14)	431.18	407.04	443.90	444.29815(32)
Δ_J (Hz)		2.079(41)				2.15(10)
Δ_{JK} (Hz)		9.59(63)				21.2(12)
Δ_K (Hz)		249.3(95)				195(16)
N_{trans}^b, N_{lines}^c		173, 107				117, 56
$J_{max}, K_{a,max}$		46, 9				42, 9
σ^d (kHz), σ_w^e		10.5, 0.85				9.7, 0.85
μ_a, μ_b (D)	5.6, 0.1		5.1, 1.1	5.3, 0.1	4.6, 1.0	

Notes. ^(a) Theoretical values of the rotational constants (see Sect. 3.3). ^(b) Total number of rotational transitions. ^(c) Total number of independent frequencies. ^(d) Standard root mean square deviation of the fit in kHz. ^(e) Weighted root mean square deviation of the fit.

tions, we derive the same column density of $(9.5 \pm 0.5) \times 10^{11} \text{ cm}^{-2}$ for 1-CNACY and 5-CNACY.

For 1- and 2-cyanonaphthalene we derive, adopting the same assumptions, a common column density of $(5.5 \pm 0.5) \times 10^{11} \text{ cm}^{-2}$. These values are a factor 1.4 times smaller than those derived by McGuire et al. (2021) for the same species. However, our identification of 1- and 2-cyanonaphthalene is based on many individual lines and a rotational temperature of 9 K, while those of McGuire et al. (2021) result from a stacking of spectral data and the assumption of four velocity components with different spatial sizes. We note that our extremely sensitive map of benzonitrile (Cernicharo et al. 2023a) does not support the spatial sizes derived from the stacking procedure. Any velocity component present in the stacked data of McGuire et al. (2021) should be present in our integrated intensity map, which indicates that benzonitrile has the same spatial distribution as many other species in TMC-1.

Assuming that the mother species, acenaphthylene and naphthalene, are ten times more abundant than their cyano derivatives, we could expect column densities for acenaphthylene ($c\text{-C}_{12}\text{H}_8$) and naphthalene ($c\text{-C}_{10}\text{H}_8$) of $\sim 10^{13} \text{ cm}^{-2}$ and $\sim 5.5 \times 10^{12} \text{ cm}^{-2}$, respectively.

Acenaphthylene itself has a small permanent dipole moment ($\mu_b = 0.31 \text{ D}$) and has been observed in the laboratory (Thorwirth et al. 2007). Only a 3σ upper limit of $N \leq 3 \times 10^{13} \text{ cm}^{-2}$ can be obtained from the QUIJOTE. This result is in line with the abundance derived from its cyano derivatives. Acenaphthene ($c\text{-C}_{12}\text{H}_{10}$, $\mu_b = 0.9 \text{ D}$) and fluorene ($c\text{-C}_{13}\text{H}_{10}$, $\mu_b = 0.53 \text{ D}$) have also been observed by Thorwirth et al. (2007). Unfortunately, only upper limits of $\sim (5\text{--}10) \times 10^{12} \text{ cm}^{-2}$ can be obtained for their column densities.

The estimated column density of acenaphthylene is larger than that of naphthalene by a factor of 1.7, which is similar to the column density ratio between indene and acenaphthylene, of namely $N = (1.6 \pm 0.3) \times 10^{13} \text{ cm}^{-2}$ (Cernicharo et al. 2021d). Hence, it seems that the growth of PAHs in TMC-1 favors the presence of PAH species containing fused five- and six-membered carbon rings. It is important to note in this context that the column density of cyclopentadiene is also significantly large, $N = (1.2 \pm 0.3) \times 10^{13} \text{ cm}^{-2}$ (Cernicharo et al. 2021d), which is of the order of the column density that can be estimated for benzene from benzonitrile (Cernicharo et al. 2022). Current chemical networks fail to explain the abundances of the simplest cycles, such as benzene and cyclopentadiene (Cernicharo et al. 2022). These latter authors examined formation routes to $c\text{-C}_5\text{H}_6$ involving cations and found that invoking the reaction between $l\text{-C}_3\text{H}_3^+$

and C_2H_4 —which measurements suggest is rapid and was found to form the cation C_5H_7^+ as a product (Smyth et al. 1982; Anicich 2003)—enabled production of the observed abundance of cyclopentadiene. That is, both neutral-neutral and ion-neutral reactions are likely to be at the origin of the growth of PAHs in cold clouds such as TMC-1. The formation of acenaphthylene itself could involve smaller rings, such as indene and naphthalene, as precursors. For example, the reaction of C_2H with naphthalene or that of C_3H with indene could directly produce acenaphthylene, although this possibility still has to be verified theoretically or/and experimentally (see Appendix F).

Acknowledgements. We thank Spanish Ministerio de Ciencia e Innovación and the European Regional Development Fund (MICINN–ERDF) for funding support through projects PID2019-106110GB-I00, PID2019-106235GB-I00, PID2021-125015NB-I00, PID2022-139933NB-I00, and PID2023-147545NB-I00. We also thank ERC for funding through grant ERC-2013-Syg-610256-NANOCOSMOS. We thank the CSIC (Spain) for funding through project PIE 2022501097. The present study was also supported by Ministry of Science and Technology of Taiwan and CSIC under the MoST-CSIC Mobility Action 2021 (Grants 11-2927-I-A49-502 and OSTW200006).

References

- Agúndez, M., Cabezas, C., Tercero, B. et al. 2021, *A&A*, 647, L10
 Agúndez, M., Cabezas, C., Fuentetaja, R. et al. 2022, *A&A*, 657, A96
 Agúndez, M., Bermúdez, C., Cabezas, C., et al. 2024, *A&A*, 688, L31
 Anderson, G. & Anderson, G. 1955. *J. Am. Chem. Soc.*, 77, 6610
 Anicich, V. G. 2003, JPL Publication 03–19
 Baba, M., Saitoh, M., Taguma, K. et al. 2009, *J. Chem. Phys.*, 130, 134315
 Becke, A. D. 1993, *J. Chem. Phys.*, 98, 1372
 Botschwina, P., Horn, M., Markey, K., & Oswald, R. 1999, *Mol. Phys.*, 92, 3
 Broadus, M. & Kass, R. 2001, *J. Am. Chem. Soc.*, 123, 4189
 Cabezas, C., Agúndez, M., Marcelino, N., et al. 2021, *A&A*, 654, L9
 Cabezas, C., Tang, J., Agúndez, M., et al. 2021, *A&A*, 676, L5
 Cabezas, C., Janeiro, J., Steber, A. L., et al. 2024, *PCCP*, 26, 23703
 Cernicharo, J., 2012, in *ECLA 2011: Proc. of the European Conference on Laboratory Astrophysics*, EAS Publications Series, 2012, Ed.: C. Stehl, C. Joblin, & L. d'Hendecourt (Cambridge: Cambridge Univ. Press), 251; https://nanocosmos.iff.csic.es/?page_id=1619
 Cernicharo, J., Marcelino, N., Agúndez, M., et al. 2020, *A&A*, 642, L8.
 Cernicharo, J., Agúndez, M., Kaiser, R., et al. 2021a, *A&A*, 652, L9
 Cernicharo, J., Agúndez, M., Cabezas, C., et al. 2021b, *A&A*, 647, L2
 Cernicharo, J., Cabezas, C., Agúndez, M. et al. 2021c, *A&A*, 647, L3
 Cernicharo, J., Agúndez, M., Cabezas, C. et al. 2021b, *A&A*, 649, L15
 Cernicharo, J., Fuentetaja, R., Agúndez, M. et al. 2022, *A&A*, 663, L9
 Cernicharo, J., Tercero, B., Marcelino, N. et al. 2023a, *A&A*, 674, L4
 Cernicharo, J., Pardo, J.R., Cabezas, C. et al. 2023b, *A&A*, 670, L19
 Cernicharo, J., Cabezas, C., Agúndez, M. et al. 2024, *A&A*, 688, L13
 Fossé, D., Cernicharo, J., Gerin, M., Cox, P. 2001, *ApJ*, 552, 168
 Frisch M. J., Pople, J. A., Binkley, J. S. 1984, *J. Chem. Phys.*, 80, 3265
 Frisch M.J., et al. 2016, Gaussian 16 Revision A.03
 Fuentetaja, R., Cabezas, C., Agúndez, M. et al. 2022, *A&A*, 663, L3
 Hahndorf, I., Lee, Y.T., Kaiser, R.I. et al. 2002, *J. Chem. Phys.*, 116, 3248

- Jena, S., Dhanalakshmi, P., Bano, G., & Thilagar, P. 2020, *J. Phys. Chem. B*, 124, 5393.
- Kaiser, R. & Hansen N. 2021, *J. Phys. Chem. A*, 125, 3826
- Kowaka, Y., Yamanaka, T. & Baba, M. 2012, *J. Chem. Phys.*, 136, 154301
- Krishnan, S. Kaden, A., Thilly, G., & Hites, A. 1979. *Environ. Sci. Tech.*, 13, 1532
- Loomis, F.W. & Wood, R.W. 1928, *Phys. Rev.*, 32, 223
- Maksyutenko, P., Zhang, F., Gu, X., & Kaiser, R.I. 2011, *PCCP*, 13 240
- McGuire, B.A., Burkhardt, A.M., Kalenskii, S., et al. 2018, *Science*, 359, 202
- McGuire, B.A., Loomis, R.A., Burkhardt, A.M., et al. 2021, *Science*, 371, 1265
- McNaughton, D., Jahn, M.K., Travers, M.J. et al. 2018, *MNRAS*, 476, 52678
- Müller, H. S. P., Schlöder, F., Stutzki, J., Winnewisser, G. 2005, *J. Mol. Struct.*, 742, 215
- Neill, J. L., Shipman, S. T., Alvarez-Valtierra, L., et al 2011, *J. Mol. Spectrosc.*, 269, 21
- Pickett H. M. 1991, *J. Mol. Spectrosc.*, 148, 371
- Pickett, H.M., Poynter, R. L., Cohen, E. A., et al. 1998, *J. Quant. Spectrosc. Radiat. Transfer*, 60, 883
- Ray, B. S. 1932, *Zeitschrift für Physik.*, 78, 74
- Silva, W. G. D. P., Cernicharo, J., Schlemmer, S., et al. 2023, *A&A*, 676, L1
- Sita, M. L., Changala, P. B., Xue, C., et al. 2022, *ApJL*, 938 , L12
- Smyth, K. C., Lias, S. G., & Ausloos, P. 1982, *Combust. Sci. Technol.*, 28, 147
- Tercero, F., López-Pérez, J. A., Gallego, J. D., et al. 2021, *A&A*, 645, A37
- Thorwirth, S., Theulé, P., Gottlieb, C. A., et al. 2007, *ApJ*, 662, 1309
- Watson, J. K. G., in "Vibration Spectra and Structure" (J. Durig, Ed.), Vol.6, p.1, Elsevier, Amsterdam, 1977
- Watson, J. K. G. 2007, *Molecular Physics*, 105, 679
- Yang, Z., Galimova, G.R., He, C. et al. 2023, *Science Advances*, 9, eadi5060

Table A.1. Fit of the $K_a=0$ lines of 1-cyanonaphthalene in the Q-band.

Transition ^a	J^* ^b	ν_{calc} ^c (MHz)	ν_{lin} ^d (MHz)	$\nu_{\text{calc}} - \nu_{\text{lin}}$ ^e (kHz)
27 _{0,27} – 26 _{0,26}	55/2	31953.900	31953.897	3.0
28 _{0,28} – 27 _{0,27}	57/2	33115.827	33115.826	1.0
29 _{0,29} – 28 _{0,28}	59/2	34277.751	34277.751	0.0
30 _{0,30} – 29 _{0,29}	61/2	35439.672	35439.672	0.0
31 _{0,31} – 30 _{0,30}	63/2	36601.589	36601.590	-1.0
32 _{0,32} – 31 _{0,31}	65/2	37763.503	37763.504	-1.0
33 _{0,33} – 32 _{0,32}	67/2	38925.413	38925.414	-1.0
34 _{0,34} – 33 _{0,33}	69/2	40087.320	40087.321	-1.0
35 _{0,35} – 34 _{0,34}	71/2	41249.222	41249.223	-1.0
36 _{0,36} – 35 _{0,35}	73/2	42411.120	42411.121	-1.0
37 _{0,37} – 36 _{0,36}	75/2	43573.014	43573.015	-1.0
38 _{0,38} – 37 _{0,37}	77/2	44734.904	44734.904	0.0
39 _{0,39} – 38 _{0,38}	79/2	45896.789	45896.789	0.0
40 _{0,40} – 39 _{0,39}	81/2	47058.669	47058.669	0.0
41 _{0,41} – 40 _{0,40}	83/2	48220.545	48220.544	1.0
42 _{0,42} – 41 _{0,41}	85/2	49382.416	49382.415	1.0

Notes. (a) Rotational quantum numbers of a -type $K_a=0$ transitions of 1-cyanonaphthalene with $K_c=J_u$. (b) Effective rotational quantum number ($J^* = J_u + 1/2$). (c) Predicted frequencies using an A -reduced Hamiltonian (representation I') and the rotational constants determined by McNaughton et al. (2018). (d) Fitted frequencies using the relation $\nu = 2B_{\text{eff}}J^* - 4D_{\text{eff}}J^{*3}$. The results of the fit are $B_{\text{eff}} = 580.987413 \pm 0.000015$ MHz and $D_{\text{eff}} = 4.9354 \pm 0.0057$ Hz. The standard deviation of the fit is 1 kHz. (e) Difference between the predicted frequencies using an A -reduced Hamiltonian (representation I') and those obtained through the linear fit with half integer quantum numbers.

Appendix A: Confirmation of the presence of cyanonaphthalenes in TMC-1

As noted in Sect. 3, we were looking for harmonic relations with half integer quantum numbers that could be related to C_7N . A dozen lines were found that, as explained in Sect. 3, could be fitted with a simple relation $\nu = 2B_{\text{eff}}J^* - 4D_{\text{eff}}J^{*3}$. These lines are shown in Fig. A.1 (lines connected with the blue line at the left). Each panel of this figure represents the data of the survey with frequencies $2B_{\text{rot}}J^*$, with J^* being $J_u + 1/2$ and J_u the integer upper quantum number of the transitions $K_a=0, 1$ of 1-cyanonaphthalene. This species has a - and b -type transitions, with similar values of the dipole moment (McNaughton et al. 2018), and has the peculiarity that the a -type $J'_{0,J''}$ – $J''_{0,J''}$ and $J'_{1,J''}$ – $J''_{1,J''}$ with $J'' = J' - 1$ collapse to the same frequency than the b -type $J'_{1,J''}$ – $J''_{0,J''}$ and $J'_{0,J''}$ – $J''_{1,J''}$. Hence, the four $K_a=0, 1$ a - and b -lines are at the same frequency which produces a natural stacking favouring the detection of these lines. These four transitions with $K_a=0,1$ will be denoted as $J' - J''(0,1)$. Examples of them are given in Fig. A.2 where the quantum numbers J' and J'' are indicated. All lines in this figure labelled as $J' - J''(n,n+1)$ correspond to two a - and two b -type collapsed transitions with upper and lower rotational quantum numbers J' and J'' , respectively.

The Ray asymmetry parameter (Ray 1932), $\kappa = (2B - A - C)/(A - C)$, of 1-cyanonaphthalene is around -0.1 , hence, the molecule is highly asymmetric. Nevertheless, a clear series of lines harmonically related appear in the diagram of Fig. A.1 as connected by a vertical line slightly tilted due to the contribution of the rotational distortion to the frequencies of the transitions. The calculated frequencies of these transitions using the rotational and distortion constants derived by McNaughton et al. (2018) are given in Table A.1, together with the fitted frequencies assuming that the lines arise from a linear molecule with half integer quantum numbers. The match between the frequencies

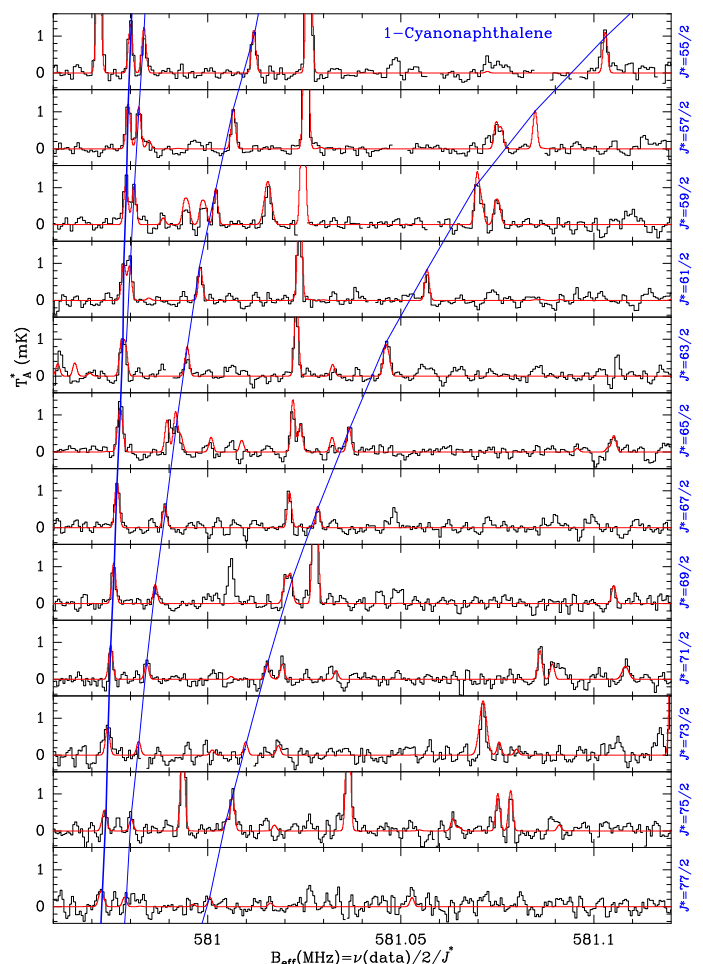


Fig. A.1. Modified Loomis-Wood diagram of some of the observed lines of 1-cyanonaphthalene. The abscissa corresponds to the value of the rotational constant. The ordinate is the antenna temperature, corrected for atmospheric and telescope losses, in milli Kelvin. Each box presents the QUIJOTE data for frequencies $2B_{\text{rot}}J^*$, where $J^* = J_u + 1/2$. The red line corresponds to the synthetic spectrum computed for TMC-1 including the rotational transitions of all molecular species detected with QUIJOTE adopting for them the physical parameters derived in previous works. Features without a red line counterpart are unknown lines. The model contains the rotational lines of the two isomers of cyanonaphthalene and cyanoacnaphthylene reported in this work. The rotational transitions of 1-cyanonaphthalene correspond to the lines connected through blue lines (see text). The left blue line corresponds to the transitions harmonically related with half integer quantum numbers ($K_a=0, 1$; a and b -type transitions; $J_u=J^*-1/2$). The other blue lines connect transitions of 1-cyanonaphthalene corresponding to $K_a=1, 2, 3$ and 4 (a and b -type).

calculated using an A -reduced Hamiltonian (representation I') for an asymmetric molecule and those obtained from a Hamiltonian for a linear molecule with half integer quantum numbers ($J^*=J_u+1/2$) is simply astonishing.

The values of B_{eff} and D_{eff} derived through the linear fit are 580.987413 ± 0.000015 MHz, and 4.9354 ± 0.0057 Hz, respectively. The parameter B_{eff} agrees extremely well with the rotational constant C derived by McNaughton et al. (2018, $C = 580.988976 \pm 0.000006$ MHz). It should be pointed out that the $K_a=0, 1$ lines cannot be reproduced with a fit to a linear species using integer quantum numbers. The additional series of lines that appear in the figure correspond to K_a values of 1, 2, 3, and 4 of a and b type. They appear connected by significantly

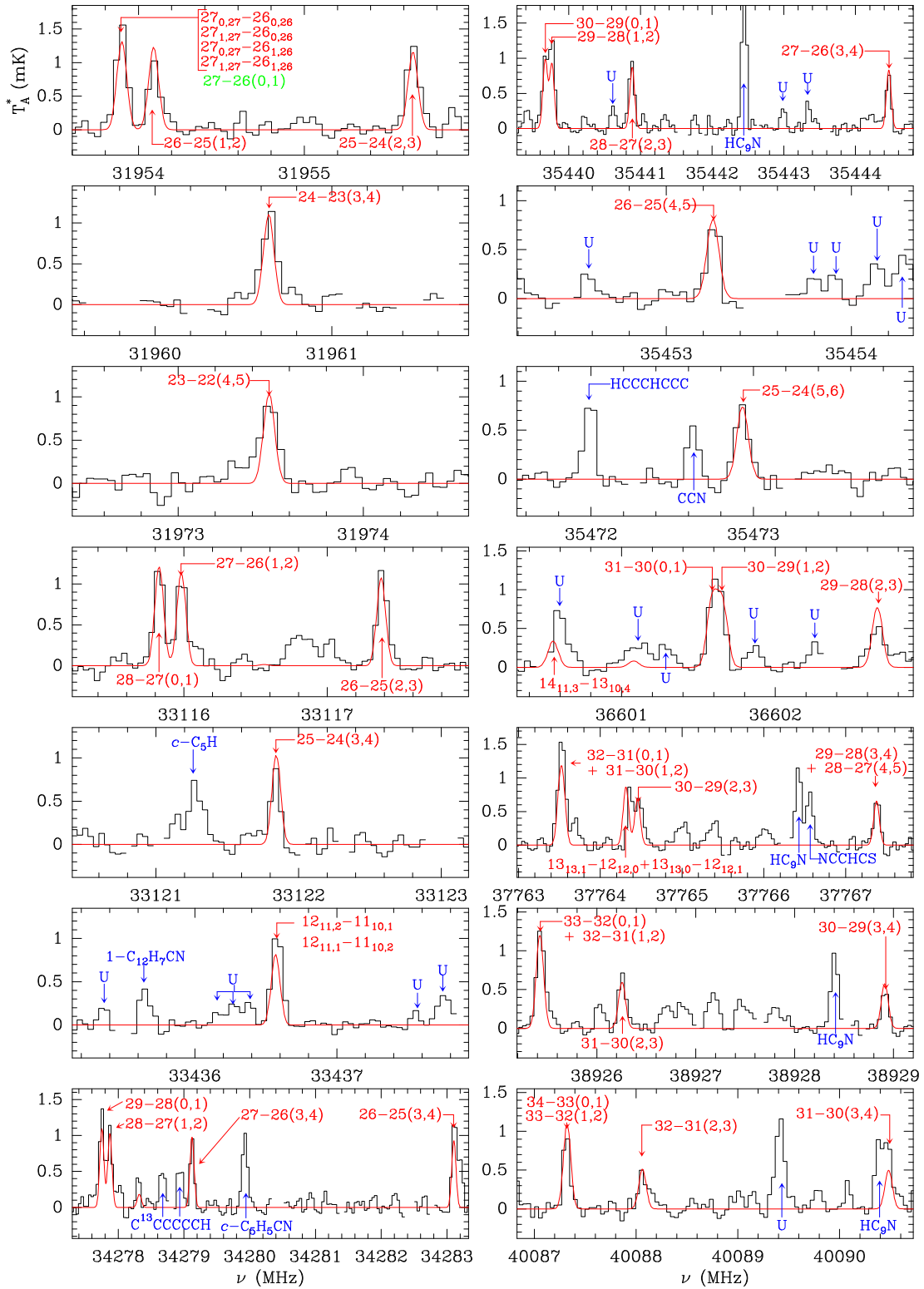


Fig. A.2. Some of the lines of Fig. A.1 over enhanced frequency scales. The lines are indicated by arrows and their quantum numbers are depicted for each feature. The red line corresponds to the synthetic spectra derived from the model presented in Sect. 4. Other lines from molecules previously studied or unknown features are indicated in blue.

curved blue lines due to the high contributions of non-diagonal terms of the Hamiltonian and of the distortion terms of the molecule. In Fig. A.2 we show a zoom for several of these lines to illustrate that they are clearly detected on a line-by-line basis. The behaviour of the $K_a = 0, 1$ lines of 1-cyanonaphthalene is the expected result for high- J values of large molecules (Watson

2007). In this case, the lines of an asymmetric top in the oblate asymptotic limit ($J=K_c$), or the prolate asymptotic limit ($J=K_a$), collapse to a single feature producing strong lines separated by $2C$ or $2A$ that appear as progressions in the spectrum. Up to four lines can be collapsed to the same frequency (see, e.g., Fig. A.2).

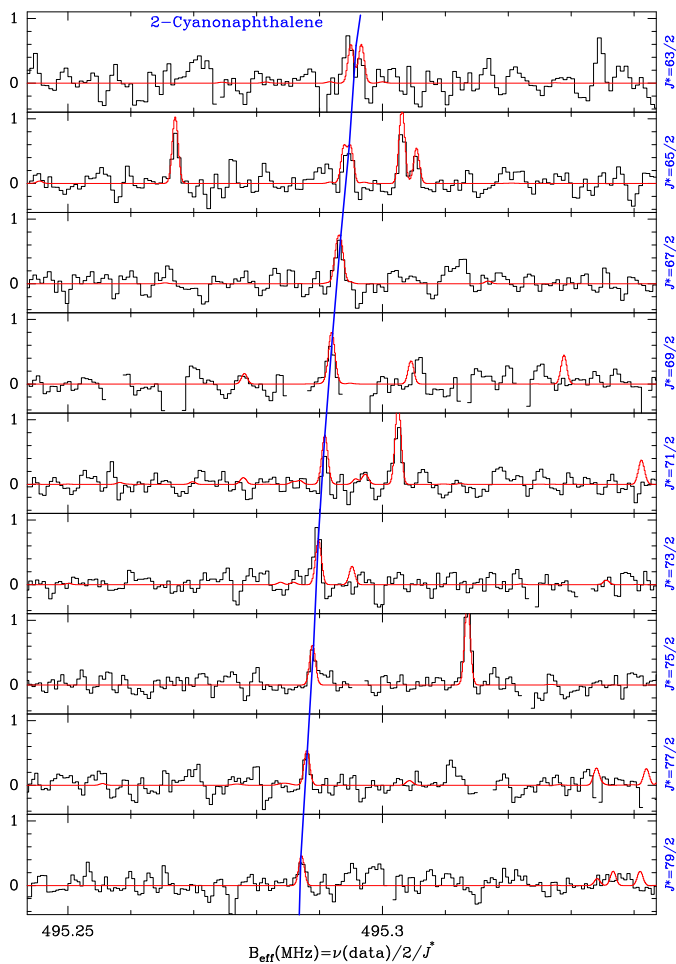


Fig. A.3. Modified Loomis-Wood diagram for the observed $K_a = 0, 1$ lines of 2-cyanonaphthalene. The abscissa corresponds to the value of the rotational constant. The ordinate is the antenna temperature, corrected for atmospheric and telescope losses, in milli Kelvin. Each box presents the QUIJOTE data for frequencies $2 B_{rot} J^*$, where $J^* = J_u + 1/2$. The red line corresponds to the synthetic spectrum computed for TMC-1 including the rotational transitions of all molecular species detected in previous works and the two isomers of cyanonaphthalene and cyanoacenaphthylene. The rotational transitions of 2-cyanonaphthalene correspond to the lines connected through the blue vertical line (see text). For this isomer of cyanonaphthalene they correspond to the a -type transitions harmonically related with half integer quantum numbers, J^* , and corresponding to $J_u = J^* - 1/2$ and $K_a = 0, 1$.

The lines of the isomer 2-cyanonaphthalene are shown in Fig. A.3. For this isomer the Ray's asymmetry parameter, κ , is -0.9 , which means that the species is near the prolate symmetric limit ($\kappa = -1$). For this isomer, the spectrum is dominated by a -type transitions, which are 25 times stronger than the b -type ones ($\mu_a = 5.2$ D, $\mu_b = 1.0$ D; McNaughton et al. 2018). For $J' = 31$ the two $K_a = 0$ and $K_a = 1$ lines are separated by 100 kHz (see top panel of Fig. A.3), while for $J' = 35$ the splitting of the two lines is only of 30 kHz and appear unresolved in our data (see panel corresponding to $J^* = 71/2$ in Fig. A.3). The a -type $J' - J''(0,1)$ lines can be reproduced with $B_{eff} = 495.317$ MHz, $D_{eff} = 13.2$ Hz, and $H_{eff} = 1.53$ μ Hz with a standard deviation of 19 kHz. A better result (5.8 kHz) is obtained by fitting an additional distortion term. The effective rotational constant using half integer quantum numbers for these $K_a = 0, 1$ transitions is very similar to the C rotational constant ($C = 495.29352$ MHz)

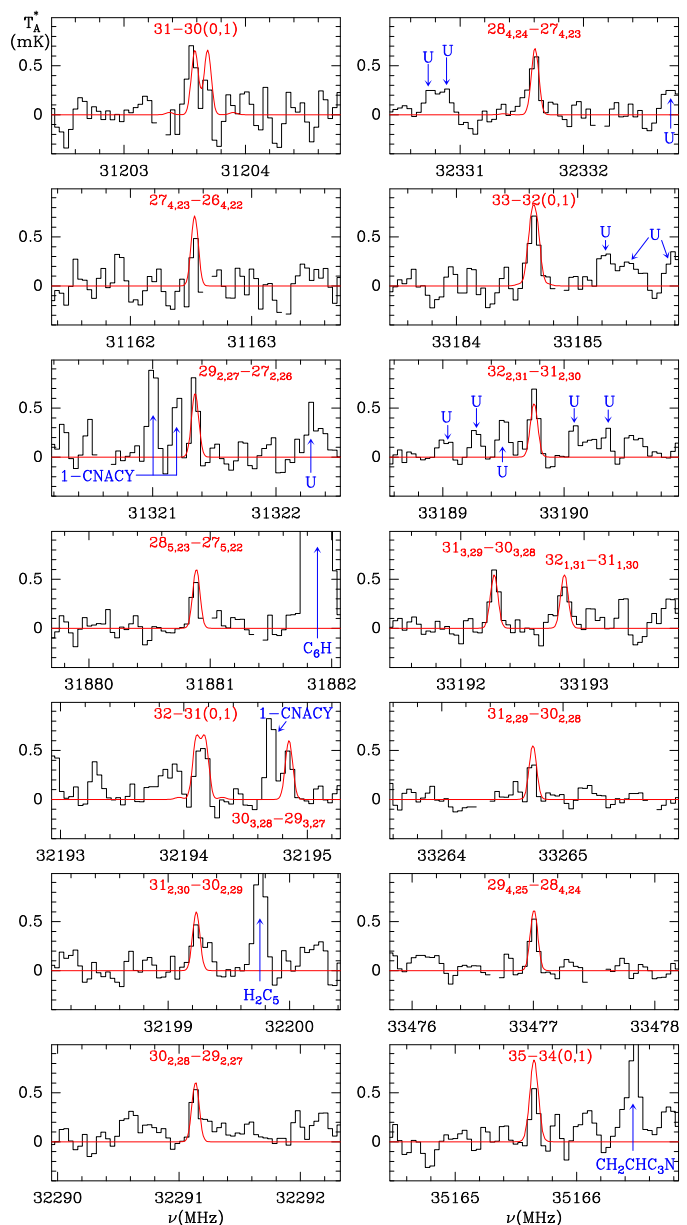


Fig. A.4. Additional lines of 2-cyanonaphthalene (see Fig. A.3). The quantum numbers are indicated for each feature. The red line corresponds to the synthetic spectra of the model for 2-cyanonaphthalene presented in Sect. 4. Other lines from molecules previously studied or unknown features are indicated in blue.

derived for this isomer by McNaughton et al. (2018). Additional lines with higher K_a values are shown in Fig. A.4.

Appendix B: Line parameters of the two CNACY isomers

Line parameters for all observed transitions with the Yebes 40m radio telescope were derived by fitting a Gaussian line profile to them using the GILDAS package. A velocity range of ± 20 km s^{-1} around each feature was considered for the fit after a polynomial baseline was removed. Negative features produced in the folding of the frequency switching data were blanked before baseline removal. A view of some of the transitions of the two isomers of CNACY is given in figures 1 and 2.

Table B.1. Observed line parameters towards TMC-1 for the two isomers of CNACY^s.

Transition	ν_{obs}^a (MHz)	Obs-Cal ^b (kHz)	$\int T_A^* dv^c$ (mK km s ⁻¹)	Δv^d (km s ⁻¹)	T_A^{*e} (mK)	Notes
1-CNACY						
36 _{0,36} – 35 _{0,35}	31321.003±0.010	–7	0.77±0.07	0.70±0.07	1.02±0.08	
36 _{1,36} – 35 _{1,35}	31321.003±0.010	–7				
35 _{1,34} – 34 _{1,33}	31321.200±0.010	–7	0.49±0.07	0.61±0.13	0.76±0.08	
35 _{2,34} – 34 _{2,33}	31321.200±0.010	–7				
34 _{2,32} – 33 _{2,31}	31322.721±0.010	–5	0.81±0.07	0.79±0.11	0.96±0.08	
34 _{3,32} – 33 _{3,31}	31322.721±0.010	–5				
33 _{3,30} – 32 _{3,29}	31327.286±0.010	2	1.00±0.09	0.78±0.05	1.20±0.06	
33 _{4,30} – 32 _{4,29}	31327.286±0.010	2				
32 _{4,28} – 31 _{4,27}	31338.050±0.010	8	0.90±0.07	0.72±0.07	1.18±0.08	
32 _{5,28} – 31 _{5,27}	31338.050±0.010	5				
31 _{6,26} – 30 _{6,25}	31361.167±0.030	6	0.85±0.08	0.80±0.00	0.99±0.12	A
31 _{5,26} – 30 _{5,25}	31361.263±0.030	–18	0.37±0.08	0.80±0.00	0.41±0.12	A
30 _{7,24} – 29 _{7,23}	31408.519±0.020	9	0.52±0.07	0.80±0.00	0.60±0.10	A
30 _{6,24} – 29 _{6,23}	31412.542±0.010	27	0.76±0.11	1.09±0.10	0.65±0.11	
28 _{9,20} – 27 _{9,19}	31424.864±0.010	22	0.74±0.09	0.90±0.12	0.77±0.10	
27 _{8,19} – 26 _{8,18}	31478.333±0.010	–4	0.68±0.07	0.96±0.15	0.66±0.08	
29 _{8,22} – 28 _{8,21}	31483.445±0.020	–1	0.55±0.10	0.96±0.18	0.54±0.11	
29 _{7,22} – 28 _{7,21}	31564.045±0.020	1	0.29±0.08	0.76±0.28	0.75±0.12	
28 _{8,20} – 27 _{8,19}	32162.846±0.010	6	0.72±0.12	0.82±0.10	0.83±0.06	
37 _{0,37} – 36 _{0,36}	32179.095±0.010	–2	0.94±0.10	0.90±0.11	0.98±0.07	
5-CNACY						
35 _{1,35} – 34 _{1,34}	31544.693±0.020	29	1.74±0.07	1.14±0.05	1.44±0.06	
34 _{1,33} – 33 _{1,32}	31544.693±0.020	–21				
35 _{0,35} – 34 _{0,34}	31544.693±0.020	29				
34 _{2,33} – 33 _{2,32}	31544.693±0.020	–21				
33 _{3,31} – 32 _{3,30}	31545.822±0.010	–10	0.53±0.05	0.83±0.10	0.60±0.06	
33 _{2,31} – 32 _{2,30}	31545.822±0.010	–10				
32 _{4,29} – 31 _{4,28}	31549.389±0.010	–3	0.97±0.05	0.80±0.05	1.14±0.06	
32 _{3,29} – 31 _{3,28}	31549.389±0.010	–3				
31 _{5,27} – 30 _{5,26}	31557.882±0.010	–9	0.83±0.12	0.93±0.16	0.84±0.06	C
31 _{4,27} – 30 _{4,26}	31557.882±0.010	–9				
30 _{6,25} – 29 _{6,24}	31576.097±0.010	–10	0.97±0.05	0.80±0.05	0.96±0.09	
30 _{5,25} – 29 _{5,24}	31576.097±0.010	–30				
29 _{7,23} – 28 _{7,22}	31613.683±0.010	–11	0.31±0.05	0.62±0.15	0.47±0.07	
29 _{6,23} – 28 _{6,22}	31614.562±0.010	–2	0.30±0.05	0.73±0.17	0.38±0.07	
28 _{8,21} – 27 _{8,20}	31685.056±0.010	15	0.41±0.07	0.62±0.13	0.63±0.09	
28 _{7,21} – 27 _{7,20}	31708.838±0.010	–9	0.21±0.07	0.83±0.26	0.24±0.07	
36 _{1,36} – 35 _{1,35}	32433.236±0.020	11	0.80±0.08	0.80±0.00	0.99±0.08	A

Notes.

^(S) The full content of this table can be found in electronic form at <https://doi.org/10.5281/zenodo.13810127>. All uncertainties correspond to 1σ .

^(a) Measured frequency assuming a v_{LSR} of 5.83 km s⁻¹ for TMC-1 (Cernicharo et al. 2020).

^(b) Observed minus calculated frequencies in kHz. The calculated frequencies are those resulting from the molecular constants obtained from a fit of an *A*-reduced Hamiltonian (representation *I'*) to the observed frequencies. The derived rotational and distortion constants are given in Table 1. Unresolved doublets are fitted to the averaged frequency of the two transitions.

^(c) Integrated line intensity (in mK km s⁻¹).

^(d) Linewidth at half intensity derived by fitting a Gaussian function to the observed line profile (in km s⁻¹).

^(e) Antenna temperature (in milli Kelvin).

^(A) Partially blended with another feature. A fixed linewidth of 0.80 km s⁻¹ has been adopted.

^(B) Only data from the observations with frequency throw of 8 MHz.

^(C) Only data from the observations with frequency throw of 10 MHz.

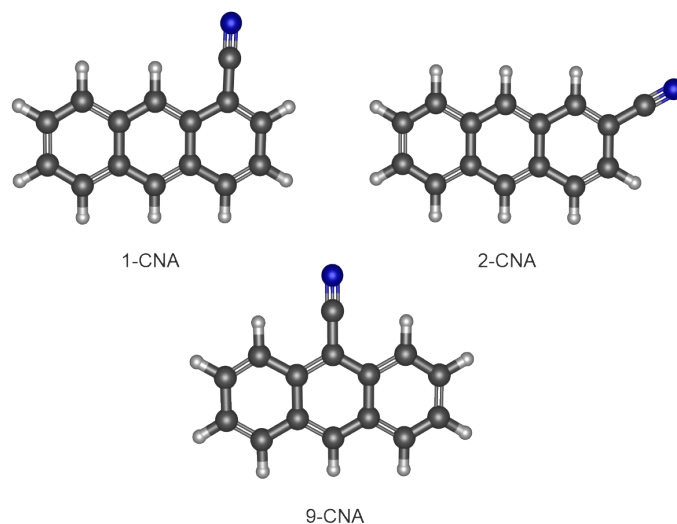
^(D) Line too broad. Probably blended with another feature. Parameters are uncertain.

^(E) Line probably blended with another feature. Parameters can be derived but are uncertain. ^(F) Narrow line. Parameters are uncertain

Table C.1. Experimental and theoretical molecular constants of acenaphthylene.

Parameter	Thorwirth et al. (2007)	Theory ^a
A (MHz)	1511.82609(12)	1513.0
B (MHz)	1220.63105(29)	1221.8
C (MHz)	675.529854(65)	675.9
Δ_J (Hz)	31.4(26)	32.77
Δ_{JK} (Hz)	-49.2(68)	-57.51
Δ_K (Hz)	20.8(44)	27.67
δ_J (Hz)	-5.4(14)	4.05
δ_K (Hz)	0.0	-12.52

Notes. ^(a) This work.

**Fig. C.1.** Chemical structure of the CNA isomers.

Appendix C: Quantum chemical calculations

Molecular geometry optimizations for all the plausible candidates were carried out using the density functional theory (DFT) variant B3LYP (Becke 1993) and the Pople triple- ζ basis set 6-311++G(d,p) (Frisch et al. 1984)). From these calculations we obtained the values of the rotational constants and those of the electric dipole moment components. In addition, for some of the candidates we also performed harmonic frequency calculations at the same level of theory. All the calculations were done using the GAUSSIAN 16 package (Frisch et al. 2016). We chose this calculation method since it reproduces fairly well the rotational constants of the PAHs and their cyano derivatives at a reasonable computational cost, as shown in McNaughton et al. (2018). See also as an example the comparative theoretical and experimental values obtained for acenaphthylene, shown in Table C.1.

We considered as plausible candidates the cyano derivatives of the PAHs with three fused rings: anthracene and phenanthrene ($c\text{-C}_{14}\text{H}_{10}$), 9*H*-fluorene ($c\text{-C}_{13}\text{H}_{10}$), acenaphthene ($c\text{-C}_{12}\text{H}_{10}$), and acenaphthylene ($c\text{-C}_{12}\text{H}_8$). In addition, we also calculated the molecular constants for the dicyano derivatives of naphthalene.

The molecular structures for all the isomers of cyanoanthracene (CNA) and cyanophenanthrene (CNP) are shown in Figs. C.1 and C.2, while the theoretical molecular constants are given in Table C.2 and C.3, together with those experimentally determined for the 9-cyanoanthracene (9-CNA) and 9-cyanophenanthrene (9-CNP) isomers, observed in the laboratory by McNaughton et al. (2018). The molecular constants for the cyano derivatives of 9*H*-fluorene (CNF) have been already published by Cabezas et al. (2024) together with the experimental constants, that are shown in Table C.4. The calculated molecular constants for the five cyano derivatives of acenaphthene (CNAC) are shown in Table C.5 and their molecular structures in Fig. C.3 and those for the acenaphthylene are summarized in Table C.1. Finally the theoretical rotational constants for the ten different dicyano derivatives of naphthalene (DCN) are shown in Table C.6 and the molecular structures in Fig. C.4.

Appendix D: Synthesis of cyanoacenaphthylene isomers

The synthesis of 1-CNACY and 5-CNACY was accomplished through short, three-step synthetic routes, starting from commercially available acenaphthene (see Figs. D.1 and D.2). Thus, benzylic dibromination of acenaphthene with NBS in the presence of benzoyl peroxide afforded 1,2-dibromoacenaphthene, which after dehydrobromination with DBU and cyanodebromination with CuCN, was converted into 1-CNACY in good yield. In contrast, treatment of acenaphthene with NBS in the absence of the radical initiator resulted in bromination at position C5, yielding 5-bromoacenaphthene in quantitative yield. Cyanodebromination followed by oxidation with DDQ afforded 5-CNACY in satisfactory yield.

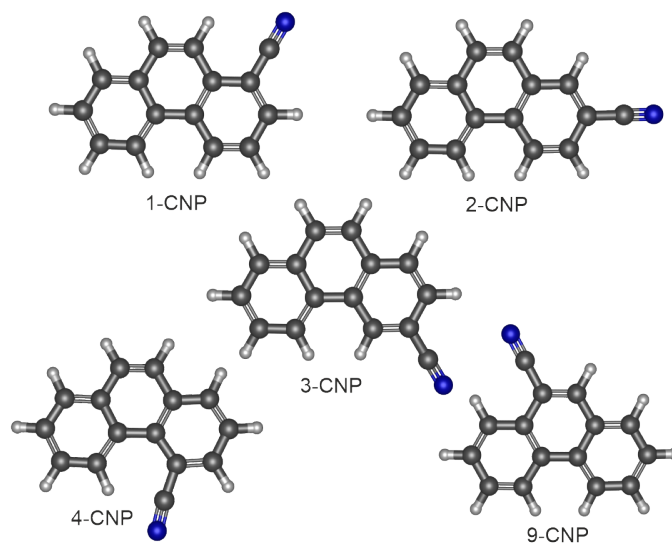


Fig. C.2. Chemical structure of the CNP isomers.

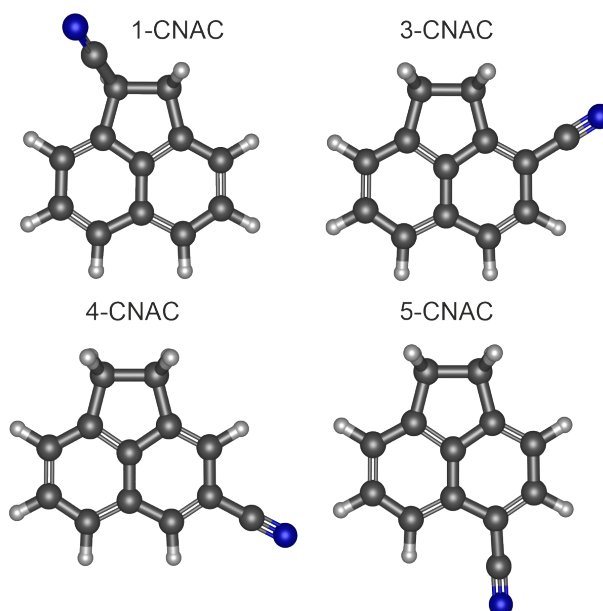


Fig. C.3. Chemical structure of the CNAC isomers.

Table C.2. Molecular constants for the CNA isomers.

Parameter	Anthracene ^a	1-CNA	2-CNA	9-CNA	9-CNA ^b
<i>A</i> (MHz)	2146.24(12)	1091.3	1845.7	985.6	985.8526447(95)
<i>B</i> (MHz)	452.540(74)	386.2	279.2	450.6	451.2051876(206)
<i>C</i> (MHz)	374.036(51)	285.2	242.5	309.2	309.6126249(178)
μ_a (D)	0.0	2.2	5.6	0.0	
μ_b (D)	0.0	4.3	1.5	4.8	

Notes. ^(a) Experimental values from Baba et al. (2009). ^(b) Experimental values from McNaughton et al. (2018).

In contrast, the 3-CNACY and 4-CNACY isomers are not accessible in a straightforward manner. In fact, they have never been prepared previously, and even the synthesis of potential precursors such as 3- or 4-bromoacenaphthylenes or -acenaphthenes would be difficult. The reason is that the reactive positions of acenaphthene are C1 (for radical reactions) and C5 (for electrophilic aromatic substitution), as shown in our synthesis. Moreover, selective functionalization of acenaphthylene in positions C3 or C4 has not been reported.

The detailed experimental procedures for the synthesis of 1-CNACY and 5-CNACY are below.

Table C.3. Theoretical molecular constants of CNP isomers.

Parameter	Phenanthrene ^a	1-CNP	2-CNP	3-CNP	4-CNP	9-CNP	9-CNP ^b
<i>A</i> (MHz)	1606.71(42)	1226.4	1610.6	1112.4	865.4	841.7	846.118706(12)
<i>B</i> (MHz)	549.672(87)	384.2	311.5	369.3	523.4	487.1	486.386496(11)
<i>C</i> (MHz)	409.552(54)	292.6	261.0	277.2	326.1	308.5	308.9368602(69)
μ_a (D)	0.0	4.1	5.7	4.6	0.2	3.7	
μ_b (D)	0.1	2.9	0.1	2.8	4.4	3.5	

Notes. ^(a) Experimental values from Kowaka et al. (2012). ^(b) Experimental values from McNaughton et al. (2018).

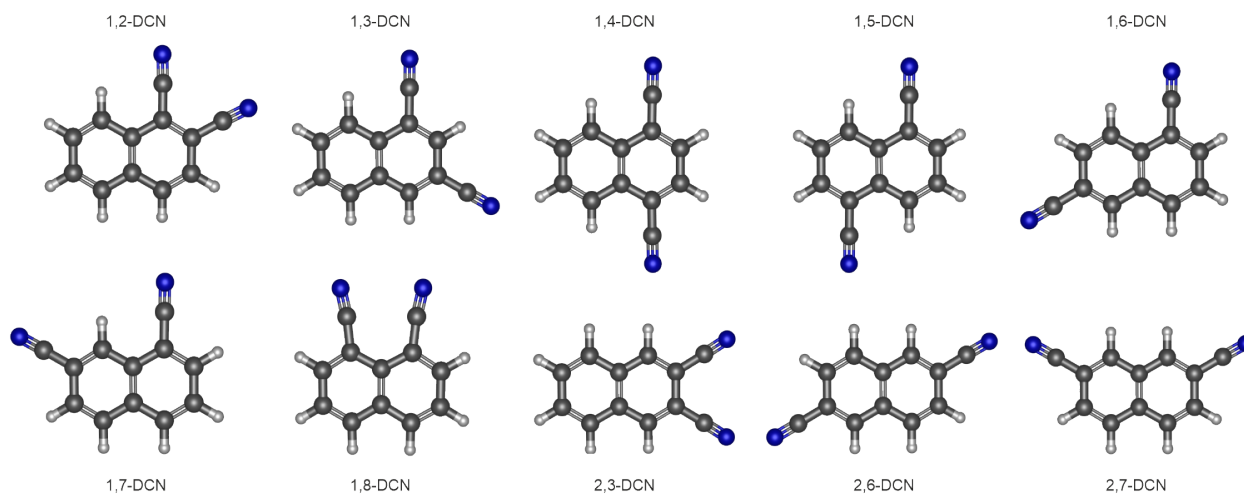
Table C.4. Experimental molecular constants of CNF isomers from Cabezas et al. (2024).

Parameter	Fluorene ^a	1-CNF	2-CNF	3-CNF	4-CNF	9-CNF
<i>A</i> (MHz)	2176.210153(70)	1303.70307(92)	2140.700(87)	1541.8327(10)	1031.74077(27)	968.61817(48)
<i>B</i> (MHz)	586.653424(70)	438.89904(23)	330.62387(37)	371.40436(23)	557.09884(28)	568.80591(40)
<i>C</i> (MHz)	463.569028(20)	329.09001(14)	286.97931(34)	299.92528(17)	362.66718(23)	373.01098(40)
Δ_J (kHz)		-	-	-	0.0206(18)	0.0359(14)
Δ_K (kHz)		-	-	-	-0.0232(21)	-
χ_{aa} (MHz)		0.213(72)	-	-2.280(39)	2.230(17)	2.229(41)
χ_{bb} (MHz)		-2.111(21)	-	0.379(24)	-4.137(13)	-2.339(18)

Notes. ^(a) Experimental values from Thorwirth et al. (2007).

Table C.5. Theoretical molecular constants of the CNAC isomers.

Parameter	1-CNAC	3-CNAC	4-CNAC	5-CNAC
<i>A</i> (MHz)	1173.8	1383.4	1362.9	1213.2
<i>B</i> (MHz)	661.6	603.0	555.3	662.7
<i>C</i> (MHz)	441.0	422.1	396.5	430.8

**Fig. C.4.** Chemical structures of the DCN isomers.**Table C.6.** Theoretical molecular constants of the DCN isomers.

Parameter	1,2-DCN	1,3-DCN	1,4-DCN	1,5-DCN	1,6-DCN	1,7-DCN	1,8-DCN	2,3-DCN	2,6-DCN	2,7-DCN
<i>A</i> (MHz)	1361.2	1004.1	1069.8	1354.3	1446.9	1111.8	935.6	1537.7	2620.8	1841.7
<i>B</i> (MHz)	566.7	600.7	642.6	556.9	471.3	571.9	826.1	476.0	349.2	381.6
<i>C</i> (MHz)	400.1	375.8	401.4	394.5	355.5	377.6	438.7	363.5	308.2	316.1
μ_a (D)	7.0	4.1	0.0	0.0	2.1	4.1	8.6	8.8	0.0	0.0
μ_b (D)	3.7	3.9	1.3	0.0	4.0	6.4	0.0	0.0	0.0	4.4

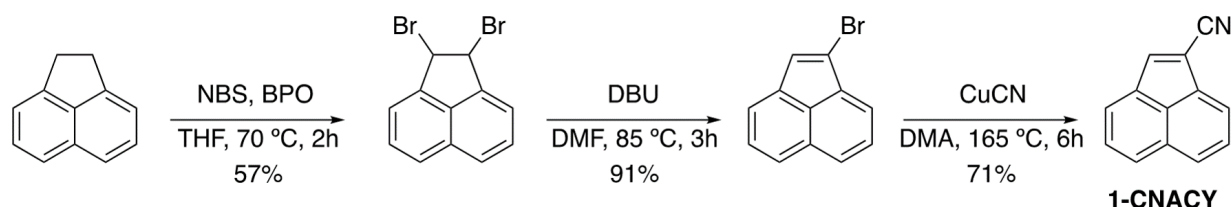


Fig. D.1. Synthesis of 1-CNACY.

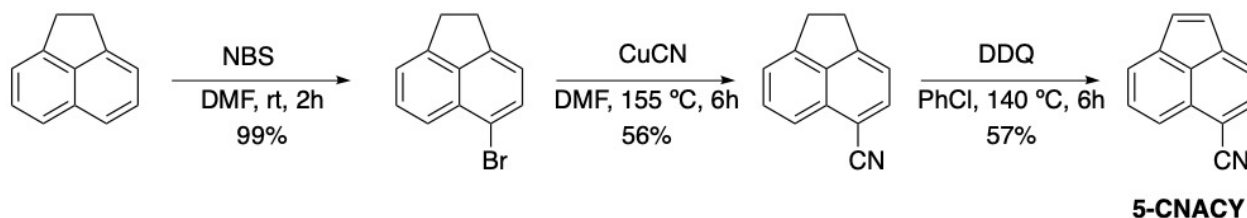


Fig. D.2. Synthesis of 5-CNACY.

D.1. Experimental procedures and characterization data

1-CNACY and 5-CNACY were synthesized according to adapted literature procedures (Anderson & Anderson 1955; Krishnan et al. 1979; Broadus & Kass 2001; Jena et al. 2020). All reactions were carried out under argon using oven-dried glassware. Anhydrous THF and DMF were taken from a MBraun SPS-800 Solvent Purification System. 1-Cyanoacenaphthylene and 5-cyanoacenaphthylene were prepared following a published procedure. Other commercial reagents were purchased from ABCR GmbH, Sigma-Aldrich or Fluorochem, and were used without further purification. TLC was performed on Merck silica gel 60 F₂₅₄ and chromatograms were visualized with UV light (254 and 360 nm). Column chromatography was performed on Merck silica gel 60 (ASTM 230-400 mesh). Centrifugation was performed in a Hettich EBA21 centrifuge. ¹H and ¹³C NMR spectra were recorded at 300 and 75 MHz (Varian Mercury-300 instrument), 400 and 101 MHz (Varian Inova 400) or 500 and 125 MHz (Varian Inova 500) respectively. Low resolution mass spectra (EI) were obtained at 70 eV on a HP-5988A instrument, while high-resolution mass spectra (HRMS) were obtained on a Micromass Autospec spectrometer. Atmospheric pressure chemical ionization (APCI) HRMS were obtained on a Bruker Microtof, using Direct Inlet Probe (DIP).

D.1.1. Synthesis of 1,2-dibromo-1,2-dihydroacenaphthylene

To a stirred solution of acenaphthylene (500 mg, 3.24 mmol) and NBS (1.32 g, 7.45 mmol) in CHCl₃ (6.5 mL), benzoyl peroxide (BPO, 78.5 mg, 0.32 mmol) was added, and the mixture stirred at reflux for 2h. Solid succinimide was filtered and the filtrate was evaporated under reduced pressure. The crude product was purified by column chromatography (SiO₂, hexane) affording 1,2-dibromo-1,2-dihydroacenaphthylene as a yellow solid (575 mg, 57%). ¹H-NMR (300 MHz, CDCl₃), δ: 7.82 (dd, *J* = 6.7, 2.3 Hz, 2H), 7.67-7.59 (m, 4H), 6.01 (s, 2H) ppm. ¹³C-NMR-DEPT (75 MHz, CDCl₃), δ: 140.51(2xC), 134.83 (C), 130.99 (C), 128.84 (2xCH), 125.86 (2xCH), 122.55 (2xCH), 54.91 (2xCH) ppm. HRMS (APCI-DIP-TOF) for C₁₂H₈Br₂ ([M⁺]) Calcd.: 308.8909; Found: 309.8911.

D.1.2. Synthesis of 1-bromoacenaphthylene

A mixture of 1,2-dibromo-1,2-dihydroacenaphthylene (500 mg, 1.6 mmol) and DBU (292.8 mg, 1.92 mmol) in DMF (32 mL) was stirred at 85 °C for 4h. Once the mixture reached room temperature it was poured in ice water, extracted with Et₂O (3x25mL) and the combined organic layers were washed with 1M HCl (15mL) and saturated NaHCO₃ (15 mL), dried over Na₂SO₄, filtered and concentrated under reduced pressure. The crude product was purified by column chromatography (SiO₂, hexane) affording 1-bromoacenaphthylene as a brown solid (323 mg, 91%). ¹H-NMR (300 MHz, CDCl₃), δ: 7.87 (d, *J* = 8.0 Hz, 1H), 7.78 (d, *J* = 8.2 Hz, 1H), 7.70 (d, *J* = 6.9 Hz, 1H), 7.61 (t, *J* = 7.4 Hz, 2H), 7.53-7.47 (m, 1H), 7.15 (s, 1H) ppm. ¹³C-NMR-DEPT (75 MHz, CDCl₃), δ: 138.22 (C), 137.98 (C), 128.94 (C), 128.89 (CH), 128.49 (CH), 127.94 (CH), 127.67 (C), 127.63 (CH), 127.04 (CH), 123.65 (CH), 123.47 (CH), 120.73 (C) ppm. HRMS (APCI-DIP-TOF) for C₁₂H₈Br ([M⁺H⁺]) Calcd.: 230.9804; Found: 230.9796.

D.1.3. Synthesis of 1-CNACY.

A mixture of 1-bromoacenaphthylene (294 mg, 1.27 mmol) and CuCN (228 mg, 2.54 mmol) in 1.3 mL of DMA was stirred at reflux for 6h. After the mixture reached room temperature, CH₂Cl₂ was added, and the resulting precipitate was filtered and washed with CH₂Cl₂. The filtrate was washed with water (15 mL) and dried over Na₂SO₄ and concentrated under reduced pressure. The crude product was purified by column chromatography (SiO₂, hexane/CH₂Cl₂ 4:1) affording 1 as a red solid (146 mg, 69%). ¹H-NMR (300 MHz, CDCl₃), δ: 8.04 (d, *J* = 8.2 Hz, 1H), 7.99-7.91 (m, 3H), 7.74 (s, 1H), 7.71-7.65 (m, 2H) ppm. ¹³C-NMR-DEPT (75 MHz, CDCl₃), δ: 139.82 (CH), 136.19 (C), 136.10 (C), 130.83 (CH), 129.23 (CH), 128.53 (CH), 128.43 (C), 128.28 (CH), 128.10 (CH).

(CH), 127.23 (C), 124.71 (CH), 115.89 (C), 111.34 (C).ppm. **HRMS (APCI-DIP-TOF)** for $C_{13}H_7N$ ($[M^+H^+]$) Calcd.: 178.0651; Found: 178.0655.

D.1.4. Synthesis of 5-bromoacenaphthene

To a stirred solution of acenaphthene (2 g, 12.96 mmol) in dry DMF (13 mL), NBS (2.33 g, 13.13 mmol) was added in three portions and the mixture stirred at room temperature for 2 h. After that, the mixture was then transferred to a flask with ice-cold water. The precipitate was filtered and washed with H_2O and dried under vacuum affording 5 as a white solid (3 g, 99%). **1H -NMR** (300 MHz, $CDCl_3$), δ : 7.77 (d, $J = 8.4$ Hz, 1H), 7.66 (d, $J = 7.3$ Hz, 1H), 7.54 (t, $J = 7.8$ Hz, 1H), 7.33 (d, $J = 7.0$ Hz, 1H), 7.13 (d, $J = 7.5$ Hz, 1H) 3.45-3.37 (m, 2H), 3.35 (m, 2H) ppm. **^{13}C -NMR-DEPT** (75 MHz, $CDCl_3$), δ : 146.22 (C), 145.93 (C), 140.28 (C), 130.93 (C), 130.88 (CH), 129.04 (CH), 121.77 (CH), 120.16 (CH), 120.03 (CH), 116.79 (C), 30.63 (CH₂), 29.91 (CH₂)ppm. **HRMS (APCI-DIP-TOF)** for $C_{12}H_9Br$ ($[M^+H^+]$) Calcd.: 232.9960; Found: 232.9959.

D.1.5. Synthesis of 5-cyanoacenaphthene

A mixture of 5-bromoacenaphthene (234 mg, 1.04 mmol) and CuCN (146.3 mg, 1.63 mmol) in DMF (3 mL) was stirred at reflux for 6h. After the mixture reached room temperature, CH_2Cl_2 was added, and the resulting precipitate was filtered and washed with CH_2Cl_2 . The filtrate was washed with water (15 mL) and dried over Na_2SO_4 and concentrated under reduced pressure. The crude product was purified by column chromatography (SiO_2 , hexane/ CH_2Cl_2 4:1) affording 5-cyanoacenaphthene as a yellow solid (100 mg, 56%) **1H -NMR** (300 MHz, $CDCl_3$), δ : 7.88 (d, $J = 8.3$ Hz, 1H), 7.85 (d, $J = 7.2$ Hz, 1H), 7.65 (dd, $J = 8.3, 7.0$ Hz, 1H), 7.44-7.42 (m, 1H), 7.32 (dt, $J = 7.2, 0.8$ Hz, 1H), 3.46 (d, $J = 1.0$ Hz, 4H) ppm. **^{13}C -NMR-DEPT** (75 MHz, $CDCl_3$), δ : 153.12 (C), 147.24 (C), 139.12 (C), 135.05 (CH), 131.39 (C), 130.87 (CH), 121.52 (CH), 120.61 (CH), 119.27 (CH), 118.55 (C), 105.21 (C), 31.34 (CH₂), 30.74 (CH₂) ppm. **HRMS (APCI-DIP-TOF)** for $C_{13}H_9N$ ($[M^+H^+]$) Calcd.: 180.0257; Found: 180.0296.

D.1.6. Synthesis of 5-CNACY.

A mixture of 5-cyanoacenaphthene (100 mg, 0.55 mmol) and DDQ (693 mg, 3.05 mmol) in dry chlorobenzene (12 mL) was stirred at reflux for 6h. After that, the solvent was evaporated under reduced pressure and the crude product was purified by column chromatography (SiO_2 , hexane/ CH_2Cl_2 4:1) affording 5-cyanoacenaphthylene (5-CNACY) as a yellow solid (56 mg, 57%). **1H -NMR** (300 MHz, $CDCl_3$), δ : 8.03-8.01 (m, 1H), 7.94 (d, $J = 7.1$ Hz, 1H), 7.74-7.62 (m, 3H), 7.18 (d, $J = 5.3$ Hz, 1H), 7.03 (d, $J = 5.3$ Hz, 1H). ppm. **^{13}C -NMR-DEPT** (75 MHz, $CDCl_3$), δ : 144.70 (C), 140.25 (C), 134.82 (CH), 133.40 (CH), 130.42 (CH), 129.50 (CH), 128.52 (C), 127.78 (C), 126.32 (CH), 125.37 (CH), 123.32 (CH), 118.03 (C), 109.54 (C) ppm. **HRMS (APCI-DIP-TOF)** for $C_{13}H_7N$ ($[M^+H^+]$) Calcd.: 178.0651; Found: 178.0651.

Appendix E: CP-FTMW spectral measurements

The experimental setup employed in this work consists of a direct-digital broadband chirped-pulse Fourier-transform microwave (CPFTMW) spectrometer (Neill et al. 2011) working over 2-8 GHz and located at the Universidad de Valladolid. The solid samples of 1-CNACY and 5-CNACY were vaporized at $\sim 120^\circ C$ in a solenoid-driven pulsed injector and diluted with an inert carrier gas (pure Ne at 2 bar). The CNACY species then expanded near adiabatically into an evacuated chamber, generating molecular jet pulses (typ. 800 μs) with effective rotational temperatures of 2 K. The molecules of each gas pulse were polarized with a series of 8 microwave chirp pulses (4 μs duration) covering the full frequency range. The measurements were performed at a repetition rate of 5 Hz, giving an effective repetition rate of 40 Hz. The chirp pulses were generated with an arbitrary waveform generator (Tektronix AWG 70002A, 25 GS/sec), amplified to 250 W with a traveling-wave tube amplifier (TWT). The excitation radiation was broadcasted perpendicularly to the jet propagation through a horn antenna. A molecular transient emission, spanning 40 μs , was then detected through a second receiving horn and amplified by a low-noise MW amplifier. A total of 1200 k FIDs per measurement were finally co-added on a digital oscilloscope (Tektronix DPO 70804C, 25 GS/sec) and a Fourier transformation finally yielded the resonance frequencies of the rotational transitions. The use of a Kaiser-Bessel apodization window produced linewidths of ca. 100 kHz. The accuracy of the frequency measurements is better than 25 kHz. All frequency components are referenced to a Rb standard.

The two CNACY isomers have high μ_a dipole moment components, 5.6 D and 4.6 D, respectively for 1-CNACY and 5-CNACY. In addition, 5-CNACY species shows a μ_b dipole moment of 1.0 D. A very rich rotational spectrum is therefore observed for both isomers (see Fig. E.1). The presence in the CNACY isomers of a ^{14}N -nitrogen nucleus, which has a nonzero nuclear spin ($I = 1$), causes each rotational transition to be split into several hyperfine components because of the nuclear quadrupole coupling effects (see Fig. E.2). Therefore, the final dataset for the 1-CNACY isomer consists of 313 hyperfine components corresponding to a -type R - and Q -branch rotational transitions with maximum values of J and K_a quantum numbers of 12 and 5, respectively. For 5-CNACY, we measured a total of 499 hyperfine components, including a - and b -type R - and Q -branch rotational transitions with maximum values of J and K_a quantum numbers of 11 and 5, respectively. All the observed hyperfine components were fitted using the SPFIT program (Pickett 1991) with the A -reduction of the Watson's Hamiltonian and III' representation (Watson 1977). We chose this fitting method since it was employed by Thorwirth et al. (2007) to fit the spectroscopic data of the acenaphthylene molecule. A combined fit of the laboratory and TMC-1 data for each isomer provides improved values for the molecular parameters. A summary of all the obtained results is shown in Tables E.1 and E.2 while all the measured transitions for 1-CNACY and 5-CNACY isomers are given in Tables E.3 and E.4. The observations corresponding to the monosubstituted ^{13}C isotopologues will be reported separately.

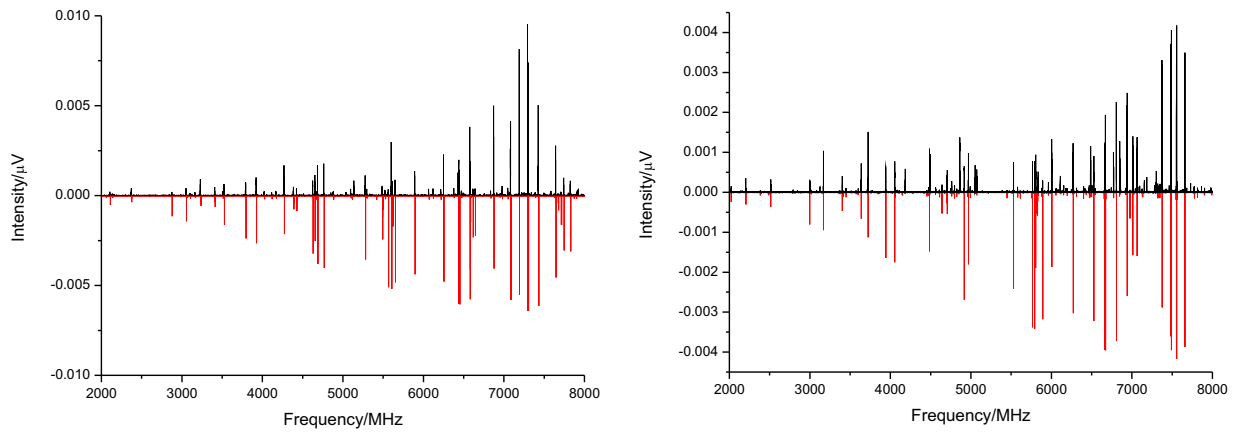


Fig. E.1. Broadband microwave spectra of 1-CNACY (left) and 5-CNACY (right) in the region 2-8 GHz. The experimental trace is represented by the positive black trace. The negative red trace is a simulation (at 2 K) using the fitted rotational parameters of Tables E.1 and E.2.

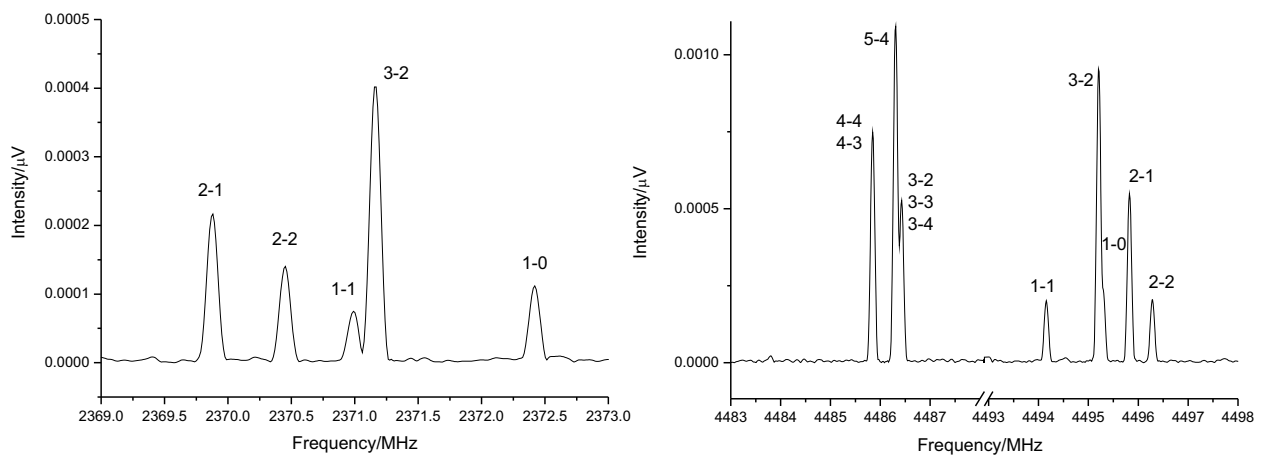


Fig. E.2. Hyperfine spectra of the $2_{1,1} - 1_{0,1}$ rotational transition of 1-CNACY (left panel) and $4_{2,3} - 3_{2,2}$ and $2_{2,0} - 1_{1,1}$ rotational transitions of 5-CNACY (right panel). Each hyperfine component is labelled with the corresponding values of quantum numbers $F'-F''$ ($F=I+J$).

The experimental molecular constants for both isomers agree very well those obtained by quantum chemical calculations. As mentioned before, we chose the III' representation. However, the values for the centrifugal distortion constants are calculated in the III' representation, and thus, the signs of the off-diagonal quartic constants, δ_J and δ_K , are reversed. This fact also occurs in the case of acenaphthylene as can be seen in the data presented in Table C.1.

Table E.1. Experimental and theoretical molecular constants of 1-CNACY.

Parameter	Laboratory(<i>III</i> ^l)	TMC-1(<i>III</i> ^l)	Lab+TMC-1(<i>III</i> ^l)	Lab+TMC-1(<i>I</i> ^r)	Theory(<i>III</i> ^r)
<i>A</i> (MHz)	1272.173002(280) ^a	1272.259(46)	1272.173142(246)	1272.173107(246)	1271.6
<i>B</i> (MHz)	647.282945(171)	647.2573(135)	647.282793(76)	647.282925(77)	647.4
<i>C</i> (MHz)	429.060379(174)	429.061350(271)	429.060651(60)	429.060554(60)	429.0
χ_{aa} (MHz)	-4.12606(280)	-	-4.12641(298)	-4.12641(298)	-4.37
χ_{bb} (MHz)	2.2166(34)	-	2.2158(36)	2.2158(36)	2.44
Δ_J (Hz)	22.33(241)	20.25(82)	21.21(133)	4.08(34)	20.44
Δ_{JK} (Hz)	9.28(225)	11.80(84)	10.61(133)	62.0(35)	11.30
Δ_K (Hz)	[-30.04] ^b	[-30.04]	[-30.04]	[-30.04]	-30.04
δ_J (Hz)	-6.21(93)	[-6.88]	-7.42(95)	1.144(171)	6.88
δ_K (Hz)	-33.21(130)	-33.03(148)	-32.04(44)	33.70(125)	32.23
<i>N</i> ^c	313	138	451	451	
σ^d (kHz)	7.2	12.0	8.7	8.7	

Notes. ^(a) The uncertainties (in parentheses) are in units of the last significant digits. ^(b) Values in brackets have been kept fix to the theoretical values. ^(c) Number of transitions included in the fit. ^(d) Standard root mean square deviation of the fit.

Table E.2. Experimental and theoretical molecular constants of 5-CNACY.

Parameter	Laboratory(<i>III</i> ^l)	TMC-1(<i>III</i> ^l)	Lab+TMC-1(<i>III</i> ^l)	Lab+TMC-1(<i>I</i> ^r)	Theory(<i>III</i> ^r)
<i>A</i> (MHz)	1246.694127(220) ^a	1246.5655(67)	1246.694215(198)	1246.694188(197)	1248.9
<i>B</i> (MHz)	690.139405(155)	690.18796(258)	690.139409(82)	690.139496(82)	688.6
<i>C</i> (MHz)	444.297616(148)	444.29786(37)	444.297766(64)	444.297706(64)	443.8
χ_{aa} (MHz)	-3.43615(258)	-	-3.43536(274)	-3.43535(274)	-3.67
χ_{bb} (MHz)	1.52992(307)	-	1.5283(32)	1.5283(32)	1.69
χ_{ab} (MHz)	-4.22(80)	-	-3.77(94)	-3.77(94)	-2.23
Δ_J (Hz)	22.05(227)	21.12(94)	20.59(123)	9.14(42)	20.80
Δ_{JK} (Hz)	-18.36(205)	-17.16(103)	-16.57(122)	17.8(35)	-16.81
Δ_K (Hz)	[-1.97] ^b	[-1.97]	[-1.97]	[-1.97]	-1.97
δ_J (Hz)	-2.48(101)	[-3.61]	-2.18(97)	3.543(206)	3.61
δ_K (Hz)	-11.85(202)	-10.22(89)	-14.31(53)	29.19(120)	12.62
<i>N</i> ^c	499	117	616	616	
σ^d (kHz)	7.7	8.8	8.8	8.8	

Notes. ^(a) The uncertainties (in parentheses) are in units of the last significant digits. ^(b) Values in brackets have been kept fix to the theoretical values. ^(c) Number of transitions included in the fit. ^(d) Standard root mean square deviation of the fit.

Table E.3. Laboratory-observed transition frequencies for 1-CNACY[§].

J'	K'_a	K'_c	F'	J''	K''_a	K''_c	F''	ν_{obs} (MHz)	Obs-Calc (MHz)
2	0	2	2	1	0	1	2	2103.611	-0.003
2	0	2	1	1	0	1	0	2103.731	-0.002
2	0	2	3	1	0	1	2	2104.897	0.012
2	0	2	1	1	0	1	1	2106.827	-0.001
2	1	1	2	1	1	0	1	2369.877	-0.001
2	1	1	2	1	1	0	2	2370.450	-0.000
2	1	1	1	1	1	0	1	2370.990	0.002
2	1	1	3	1	1	0	2	2371.162	-0.000
2	1	1	1	1	1	0	0	2372.418	-0.000
9	3	6	9	9	3	7	9	2769.378	-0.002
9	3	6	10	9	3	7	10	2769.593	-0.001
9	3	6	8	9	3	7	8	2769.593	-0.001
3	1	3	3	2	1	2	3	2873.588	-0.000
3	1	3	3	2	1	2	2	2874.204	0.003

Notes. ^(§) The full content of this table can be found in electronic form at <https://doi.org/10.5281/zenodo.13810127>.

Table E.4. Laboratory-observed transition frequencies for 5-CNACY[§].

J'	K'_a	K'_c	F'	J''	K''_a	K''_c	F''	ν_{obs} (MHz)	Obs-Calc (MHz)
2	1	2	2	1	1	1	1	2022.170	-0.001
2	1	2	2	1	1	1	2	2022.628	-0.004
2	1	2	3	1	1	1	2	2023.243	-0.001
2	1	2	1	1	1	1	0	2024.266	-0.000
2	0	2	2	1	0	1	2	2202.717	-0.000
2	0	2	1	1	0	1	0	2202.844	-0.008
2	0	2	2	1	0	1	1	2203.789	0.012
2	0	2	3	1	0	1	2	2203.789	0.012
2	0	2	1	1	0	1	1	2205.419	-0.004

Notes. ^(§) The full content of this table can be found in electronic form at <https://doi.org/10.5281/zenodo.13810127>.

Appendix F: Chemical routes for the formation of acenaphthylene

Taking into account the peculiar physical conditions of TMC-1 we have to explore barrier-less bimolecular reactions to reach the production of acenaphthylene. We describe below three different chemical routes that could be considered in the chemical networks for these large PAHs in cold dark clouds.

F.1. Formation of 1- and 5-CNACY

In this route we consider that acenaphthylene is formed first and then it reacts with cyano radicals through a barrierless addition-substitution reaction. In this case we have the question of why only 1- and 5-CNACY are formed with similar abundances and not the 3- and 4-isomers.

Acenaphthylene can be formed by four subroutes involving in principle $C_{11}+C_1$, $C_{10}+C_2$, C_9+C_3 and C_8+C_4 reactions. However, none of the C_8+C_4 reactions, $C_8H_8+C_4H$ and $C_8H_7+C_4H_2$, can form acenaphthylene.

The reactions $C_{11}+C_1$ are highly unlikely. Among two of these routes it is worth to mention the reaction of atomic carbon and methyl-naphthalene ($C_{11}H_{10}$; no yet detected in TMC-1). However, this reaction requires a loss of H_2 and an insertion of C, $C_{11}H_{10} + C \rightarrow C_{12}H_8 + H_2$. The reaction could start by the insertion of C in the CH_3 group while it is known that C attacks preferentially the aromatic rings as shown in X-beams experiments (Hahndorf et al. 2002, and references therein). Hence, although possible in principle, this pathway is very unlikely.

We could also consider the reaction between atomic carbon and the radical obtained by loss of an hydrogen of the CH_3 group of methyl-naphthalene. The reaction could be $C_{11}H_9 + C \rightarrow C_{12}H_8 + H$. As commented previously, C prefers to attack the aromatic rings and, hence, this pathway is also very unlikely.

Finally, for the $C_{10}+C_2$ path the reaction of the naphthyl radical with acetylene $C_{11}H_7+C_2H_2 \rightarrow C_{12}H_8 + H$ does form acenaphthylene, but there is a barrier which cannot be overcome under TMC-1 conditions. However, the reaction of naphthalene with the ethynyl radical (C_2H) forms on the paper acenaphthylene (along with 1- and 2-ethynyl-naphthalene), $C_{10}H_8 + C_2H \rightarrow C_{12}H_8 + H$. This reaction has to be calculated. As discussed in Sect. 4 is one of the most likely pathways to form the acenaphthylenes.

Among the reactions of $C_9 + C_3$ to consider, that of indene with C_3H which could form on the paper acenaphthylene. This reaction proceeds barrierlessly via addition of $CCCH$ either to the 6- or 5-membered rings, followed by isomerization (ring closure, H shift) and H loss to acenaphthylene ($C_9H_8 + C_3H \rightarrow C_{12}H_8 + H$). Another possible way is the reaction of the 9-indenyl radical, C_9H_7 , with the $HCCCH$ isomer of C_3H_2 . Molecular beams experiments showed that the the 9-indenyl radical can be formed easily (Yang et al. 2023); also $HCCCH$ – the non-detected C_3H_2 isomer – can also be formed easily as shown in crossed beams experiments (Maksyutenko et al. 2011). This pathway also proceeds barrierlessly via addition of $HCCCH$ either to the 6 or 5 membered ring followed by isomerization (ring closure, H shift) and H loss to acenaphthylene. These reaction has to be calculated as they are probably important formation routes of acenaphthylene (see Sect. 4).

F.2. Formation of 5-CNACY

In this route we consider that the 5-isomer is formed from 1-cyanonaphthalene which reacts with CCH (routes $C_{10} + C_2$) to form 5-CNACY. However, the 3- and 4- isomers of CNACY could be also formed in this way. However, 1-CNACY will require additional isomerization. In this route cyanonaphthalene is formed first. The reaction has to be calculated.

F.3. Formation of 1-CNACY

For 1-CNACY we could consider that naphthalene is formed first and that it reacts with $CCCN$ leading to the formation of 1-CNACY, $C_{10}H_8 + C_3N \rightarrow 1-C_{12}H_7CN + H$. This reaction has to be calculated.